Long-range transported continental aerosol in the Eastern North Atlantic: three multiday event regimes influence cloud condensation nuclei

Francesca Gallo[1*], Janek Uin[2], Kevin J. Sanchez[3], Richard H. Moore[3], Jian Wang[4], Robert Wood[5], Fan Mei[6],
Connor Flynn[7], Stephen Springston[2], Eduardo B. Azevedo[8], Chongai Kuang[2], Allison C. Aiken[1]

[1]Earth and Environmental Sciences Division, Los Alamos National Laboratory, Los Alamos, NM, USA
[2]Environment and Climate Science Department, Brookhaven National Laboratory, Upton, NY, USA
[3]NASA Langley Research Centre, Hampton, VA
[4]Center for Aerosol Science and Engineering, Department of Energy, Environmental and Chemical Engineering,
Washington University in St. Louis, St. Louis, MO, USA
[5]Department of Atmospheric Sciences, University of Washington, Seattle, USA
[6]Atmospheric Measurement and Data Sciences, Pacific Northwest National Laboratory, Richland, WA, USA
[7]School of Meteorology, University of Oklahoma, OK, USA
[8]Group of Climate, Meteorology and Global Change (CMMG), University of Azores, Portugal

*now at NASA Langley Research Centre, Hampton, VA

Correspondence to: Allison C. Aiken (aikenac@lanl.gov), Francesca Gallo (francesca.gallo@nasa.gov)

Abstract.

The Eastern North Atlantic (ENA) is a region dominated by pristine marine environment and subtropical marine boundary layer clouds. Under unperturbed atmospheric conditions, the regional aerosol regime at ENA varies seasonally due to different seasonal surface-ocean biogenic emissions, removal processes, and meteorological regimes. However, during periods when the marine boundary layer aerosol at ENA is impacted by particles transported from continental sources, aerosol properties within the marine boundary layer change significantly, affecting the concentration of cloud condensation nuclei. Here, we investigate the impact of long-range transported continental aerosol on the regional aerosol regime at ENA using data collected at the U.S. Department of Energy's (DOE) Atmospheric Radiation Measurement (ARM) User Facility on Graciosa Island in 2017 during the Aerosol and Cloud Experiments (ACE-ENA) campaign. We develop an algorithm that integrates number concentrations of particles with optical particle dry diameter (D_p) between 100 and 1000 nm, single scattering albedo, and black carbon concentration to identify multiday events (with duration > 24 consecutive hours) of long-range continental aerosol transport at ENA. In 2017, we detected nine multiday events of long-range transported particles that correspond to ~7.5% of the year. For each event, we perform HYSPLIT 10-day backward trajectories analysis, and we evaluate CALIPSO aerosol products to assess respectively origins and compositions of aerosol particles arriving at ENA. Subsequently, we group the events into three categories 1) mixture of dust and marine aerosols from North Africa, 2) mixture of marine and polluted continental aerosols from industrialized areas, and 3) biomass burning aerosol from North America and Canada, and we evaluate their influence on aerosol population and cloud condensation nuclei in terms of potential activation fraction and concentrations at supersaturation of 0.1% and 0.2%. The arrival of dust and marine aerosol mixture plumes at ENA in the winter caused significant increases in N_{tot}. Simultaneously, the particle size modes and CCN potential activation fraction remained almost unvaried, while cloud condensation nuclei concentrations increased proportionally to N_{tot}. Events dominated by mixture of marine and polluted continental aerosols in spring, fall, and winter led to statistically significant increase in N_{tot}, shift towards larger particular sizes, higher CCN potential activation fractions, and cloud condensation nuclei concentrations > 170% and up to 240% higher than during baseline regime. Finally, the transported aerosol plumes characterized by elevated concentration of biomass burning aerosol from continental wildfires detected in the summertime did not statistically contribute to increase aerosol particle concentrations at ENA. However, particles diameters were larger than under baseline conditions

and CCN potential activation fractions was > 75% higher. Consequentially, cloud concentration nuclei concentrations increased ~115% during the period affected by the events. Our results suggest that, through the year, multiday events of long-range continental aerosol transport periodically affect ENA and represent a significant source of CCN in the marine boundary layer. Based on our analysis, in 2017, the multiday aerosol plume transport events at ENA caused a total N_{CCN} increase at SS

5   0.1% of ~22% (23% at SS 0.2%) being 6.6% (6.5% at SS 0.2%), 8% (8.2% at SS 0.2%), and 7.4% (7.3% at SS 0.2%) respectively the contribution attributable to plumes dominated by mixture of dust and marine aerosols, mixture of marine and polluted continental aerosols, and biomass burning aerosols. Changes in baseline N_{tot} and particle size modes during the events might be used as a proxy to estimate the contribution to N_{CCN}.

10   **1 Introduction**

Atmospheric aerosols are one of the key components of the climate system interacting with clouds and affecting cloud radiative properties, height, and water content (Twomey, 1974; Albrecht, 1989). Remote marine low-lying cloud regions are thought to be the most affected by changes in aerosol properties because clouds are optically thin and the background aerosol concentration is low (Moore et al., 2013; Rosenfeld et al., 2014; Wood et al., 2015). However, the interactions among marine

15   boundary layer (MBL) aerosol number concentration (N_{tot}), cloud condensation nuclei (CCN) and cloud droplet concentration under different aerosol loading are still poorly understood and remain one of the largest sources of uncertainties in climate models and future climate projections (Bony, 2005; Carslaw et al., 2013; Fan et al., 2016; Seinfeld et al., 2016).

Over the past years, an increased number of studies and field campaigns have been dedicated to remote marine low-clouds systems in the North Atlantic Ocean to improve the parametrization of aerosol and cloud processes in the MBL (Albrecht et

20   al., 1995; Rémillard et al., 2012; Wood et al., 2015; Behrenfeld et al., 2019; Sorooshian et al., 2020; Redemann et al., 2021; Wang et al., 2021). The observations collected have provided invaluable insights into the potential role of aerosols in controlling cloud properties and precipitation. Namely, perturbations in aerosol properties have been found to be associated with strong synoptic meteorological variability (Rémillard et al., 2012), variations in CCN number concentrations (N_{CCN}) and cloud optical depth (Liu et al., 2016), and increases in larger longer lasting cloud cover, precipitation suppression, and cooling

25   (Rosenfeld et al., 2014). Further efforts have been focused on examining the influence of long-range transport of continental particles on unperturbed aerosol marine regimes. These studies underline the potential of long-range transported aerosols of continental origins to alter the concentration of aerosols, cloud condensation nuclei, cloud droplets and efficiency of precipitation formation (Garrett and Hobbs, 1995; Dadashazar et al., 2021; Tomlin et al., 2021; Wang et al., 2021). Despite the importance of this topic, a quantitative understanding of the cloud condensation nuclei budget changes over the North

30   Atlantic Ocean as a function of aerosol perturbations due to continental emissions is still missing and the aerosol indirect forcing remains uncertain (Carslaw et al., 2013).

With the goal of characterizing aerosol and cloud interactions in extratropical marine environments, in 2013, the U.S. Department of Energy's (DOE) Atmospheric Radiation Measurement (ARM) User Facility established a long-term fixed site Facility in the Eastern North Atlantic (ENA) (Mather and Voyles, 2013; Dong et al., 2014; Logan et al., 2014; Feingold and

35   McComiskey, 2016), in the Azores Archipelago. The ENA ARM site is located on the remote Graciosa Island, one of the smallest and least populated islands of the archipelago. Variations in synoptic meteorological conditions and the entrainment of transported continental aerosol particles from the free troposphere into the marine boundary layer periodically affect the local conditions in the Archipelago throughout the year. These features make the ENA ARM site well-suited for collecting open ocean representative measurements, and an excellent location to investigate the impact of long-range transport of

40   continental particles on low-cloud systems in pristine marine regions (Wood et al., 2015; Wang et al., 2021).

The ENA Facility includes an Aerosol Observing System (AOS) for the continuous measurements of aerosol physical, optical, and chemical properties, and the associated meteorological parameters at time resolutions from seconds to minutes (Uin et al., 2019). In situ AOS observations provide an unprecedented opportunity to robustly study the interaction between aerosols and clouds to achieve a quantitative understanding of the key controlling processes that drive aerosol properties and the CCN

5   budget in the MBL. In addition to the AOS routine measurements, during two Intensive Operating Periods (IOPs) (June-July 2017 and January-February 2018) of the ARM Aerosol and Cloud Experiments in the Eastern North Atlantic (ACE-ENA) field campaign, the ARM Aerial Facility (AAF) Gulfstream-159 (G-1) research aircraft flew over the ENA site and provided in-situ characterizations of the marine boundary layer and lower free troposphere structure, as well as the vertical distribution and horizontal variability of low clouds and aerosols (Wang et al., 2021). High correlation (slope = 1.04 +/- 0.01, r^2 = 0.7)

10   between AOS submicron number concentrations of particles at the ENA fixed site and AAF measurements were found during the summer indicating the broader regional representativeness of the AOS surface measurements when the boundary layer is well mixed (Gallo et al., 2020).

In this study, we leverage the AOS datasets collected at ENA during 2017 to constrain the influence of long-range transported particles with different continental origins on the cloud condensation nuclei concentrations in pristine marine environment.

15   First, we develop an algorithm that integrates aerosol property indicators of the presence of continental particles to detect multiday (> 24 consecutive hours) transported aerosol plume events at ENA. Changes in specific aerosol properties caused by the arrival of continental air masses over the ENA region have been described in previous literature. Namely, increased concentrations of submicron aerosol particles have been reported in the Western and Eastern North Atlantic by a number of previous studies (Garrett and Hobbs, 1995; Logan et al., 2014; Pennypacker and Wood, 2017; Sanchez et al., 2022).

20   Simultaneously, elevated levels of black carbons (BC) and low submicron single scattering albedo (SSA) values in different locations in the North Atlantic region have been associated with the presence of continental air masses containing products from incomplete fossil fuel combustion and biomass burning (Kleefeld, 2002; Junker et al., 2006; Costabile et al., 2013; O'Dowd et al., 2014; China et al., 2015; Cavalli et al., 2016). Based on these studies, we develop our algorithm and define specific thresholds for each of the aerosol parameters discussed above to detect periods affected by continental air masses

25   (Section 2.2).

Once the multiday aerosol plume transport events have been detected by the algorithm, we assess aerosol regimes at ENA under both regional aerosol baseline conditions (Sect. 3.1) and during period of times impacted by the arrival of continental aerosol particles (Sect. 3.2). Namely, we first evaluate aerosol sources and sinks under unperturbed marine conditions providing the necessary framework to understand the influence of continental transport on marine aerosol population and CCN

30   budget. Subsequently, we determine the origins and types of aerosols transported at ENA during the multiday events using Hysplit backward trajectories and Cloud-Aerosol Lidar and Infrared Pathfinder Satellite Observations (CALIPSO) classification respectively, and we present three case studies representatives of the diverse continental aerosol plumes arriving at ENA through the year: mixture of dust and marine aerosols (Sect. 3.2.1), mixture of polluted continental and marine aerosols (Sect. 3.2.2), and biomass burning aerosols (Sect. 3.2.3). In addition, we provide a summary statistic of multiday aerosol plume

35   transport event influences on aerosol physical properties, such as variation in particle number concentrations and shifts in size distribution, and CCN potential activation factor and concentrations at ENA (Sect 3.2.4).

2 Measurements and methodology

2.1 ENA ARM facility

40   Measurements of *in situ* aerosol properties examined in this study were collected though the Aerosol Observing System (AOS)

at the ENA ARM fixed facility on Graciosa Island (39° 5' 28" N, 28° 1' 36" W), approximately 10 m above ground level (Bullard et al., 2017; Uin et al., 2019), between January 1st, 2017 and December 31st, 2017. A list of the AOS measurements analyzed here, including references for each instrument, is given in Table 1 and summarized in the following sections.

Prior to conducting any data analysis, periods impacted by local aerosol events were removed from submicron aerosol number

5   concentration (N_{tot}), size distribution, single scattering albedo, black carbon, and cloud condensation nuclei datasets using the ENA-Aerosol Mask algorithm specifically developed for the AOS measurements at ENA (Gallo et al., 2020).

2.1.1 Aerosol physical properties

Measurement of submicron particle number concentrations (N_{tot}) with optical particle diameter (D_p) > 10 nm are made with a Condensation Particle Counter (CPC) Model 3772 (TSI, Inc., Shoreview, MN, USA) (Kuang et al., 2019). A Ultra-High

10 Sensitivity Aerosol Spectrometer (UHSAS) (Droplet Measurement Technologies, Inc., Longmont, CO, USA) is used for sizing particles with D_p between 70 and 1000 nm (Uin, 2016b). Size distributions of submicron aerosol particles are described by separating the data into three size modes: 1) Aitken (At) mode aerosols with $D_p \leq 100$ nm, 2) Accumulation (Ac) mode aerosols with D_p between 100 and 300, and 3) Large Accumulation (LA) mode aerosol with D_p between 300 and 1000. The number concentration of the Accumulation (N_{Ac}) and Large Accumulation (N_{LA}) modes aerosol are directly measured by the

15 UHSAS, while CPC and UHSAS measurements are combined to calculate the Aitken (N_{At}) mode as the difference between total particle number concentrations and the sum of the two larger modes: $N_{At} = N_{tot} - (N_{Ac} + N_{LA})$. Number concentrations of cloud condensation nuclei (N_{CCN}) are measured using a Cloud Condensation Nuclei (CCN) Counter (Droplet Measurements Technologies Inc.) at five levels of supersaturations from 0.1% to 1% (Roberts and Nenes, 2005; Rose et al., 2008). Here, we utilize CCN measurements collected at the determined supersaturation (SS) levels of 0.1% and 0.2% which represent typical

20 maximum supersaturations in marine boundary layer clouds where CCN activation occurs (Korolev and Mazin, 2003; Clarke and Kapustin, 2010; Wood, 2012). Furthermore, we combine CPC and CCN measurements to calculate the aerosol potential activation fraction (AF) as the ratio of N_{CCN} to the total submicron aerosol number. Finally, the hygroscopicity of aerosol particles with initial dry size from 50 to 250 nm is measured using a Humidified Tandem Differential Mobility Analyzer (HTDMA) (Brechtel Manufacturing, Inc.). Particle hygroscopic growth (HG) at subsaturated conditions is calculated as the

25 ratio of the geometric mean mobility diameter of the humidified particles (d_m(RH)) (RH > 85%) to the dry diameter (d_d). According to the kappa-Köhler Theory (Petters and Kreidenweis, 2007) and using HG, we calculate the hygroscopicity parameter κ for dry particles with $D_p = 50, 100, 150, 200,$ and 250 nm as:

$$\kappa = (HG^3 - 1)\left[\frac{\exp\left(\frac{A}{HG\, d_d}\right)}{RH} - 1\right]$$

where A is the Kelvin parameter defined as:

30 $A = \frac{4\,\sigma_w\,M_w}{RT\,\rho_w}$

M_w, σ_w and ρ_w are, respectively, the molar mass, the surface tension and the density of the water. R is the universal gas constant and T is the temperature. The instrument and its mode of operation are described in detail by (Lopez-Yglesias et al., 2014).

2.1.2 Optical properties and black carbon

35 Aerosol absorption coefficients (B_{abs}) are measured at ENA using a three-wavelength Particle Soot Absorption Photometer (PSAP) at λ of 464, 529, and 648 nm. The instrument is described in detail by Bond et al. (1999) and Virkkula et al. (2005). The response of the PSAP is affected by mass flow calibration, filter loading, amount of light scattered by the particles, the flow rate, and the spot size of the sample (Bond et al., 1999; Virkkula et al., 2005; Virkkula, 2010). ARM archive PSAP data includes corrections for the mass flow calibration and filter loading (Springston, 2018). Aerosol scattering coefficients (B_{sca})

at ENA are measured at λ of 450, 550, and 700 nm using a TSI Integrating Nephelometer (TSI, model 3563). The B_{sca} at 450 nm was scaled to the measured B_{abs} λ of 464 through interpolation based on Scattering Angstrom Exponent (SAE) (Costabile et al., 2013). In this study we use aerosol light absorption (B_{abs}) and scattering (B_{sca}) coefficients to calculate the single scattering albedo (SSA) at 464 nm defined as SSA = (B_{sca}) / (B_{abs} + B_{sca}). Equivalent black carbon (BC) concentrations are

5 estimated from (B_{abs}) with an assumed mass absorbing cross section of 6.4 m^2 g^{-1} at 648 nm (Bond and Bergstrom, 2006).

2.2 Multiday transported aerosol plume event identification algorithm and statistical analysis

We develop an algorithm to detect multiday transported aerosol plume events, which relies on the variations of physical and optical aerosol properties caused by long-range transport of particles in the Eastern North Atlantic. The application of the algorithm requires continuous measurements of the following three parameters: number concentrations of particles with optical

10 particle dry diameter (D_p) between 100 and 1000 nm, submicron SSA at at 464 nm wavelength, and black carbon concentration. The measurements are averaged over 6-hour periods and the thresholds for the three aerosol parameters are established based on earlier works conducted in the Eastern North Atlantic region that describe their variations during the period affected by transport of continental air masses. Namely, Pennypacker and Wood (2017) observed at ENA daily median number concentrations of D_p 100 to 1000 nm particles above 100 cm^{-3} during periods dominated by high sea-level pressure and large-

15 scale subsistence with air masses originating from North America approaching the Azores from the northwest. In the same study, the high median concentration of particles D_p 100-1000 nm regime was found to be associated with median and 75th percentile SSA values of 0.92 and 0.95 respectively, at 470 nm wavelength. Black carbon concentrations ranging between 10 and 40 ng m^{-3} during clean conditions have been reported by field studies conducted in different locations in the North Atlantic (O'Dowd et al., 2004; Shank et al., 2012; Pohl et al., 2014; Cavalli et al., 2016) and a threshold of 75 ng m^{-3} has been typically

20 utilized to indicate the presence of continental influenced air masses (Cooke et al., 1997; Kleefeld, 2002; Junker et al., 2006). In more recent works, Facchini et al. (2008), O'Dowd et al. (2014), and Saliba et al. (2020) have used BC 50 ng m^{-3} as a threshold value to identify combustion influences at Mace Head. Based on this literature, the algorithm flags the data as affected by long-range transported aerosols when the following conditions occur at the same time for at least 24 consecutive hours (four consecutive 6-hours periods): 1) median number concentration of D_p 100 - 1000 nm particles > 100 cm^{-3} over 6 hours period,

25 2) median submicron single scattering albedo at λ 464 nm < 0.95, and 3) mean black carbon concentrations > 40 ng m^{-3}.
Once the multiday transported aerosol plumes events are detected, their origins and transport paths are evaluated by performing 10-day backward trajectories arriving at 50 m and 500 m above the ENA site. The analysis are conducted using the Hybrid Single-Particle Lagrangian Integrated Trajectory (HYSPLIT) 4 model (Stein et al., 2015) with a time step of 6 hours using National Center Environmental Prediction (NCEP) Global Data Assimilation System (GDSA) meteorological data and model

30 vertical velocity as input. In addition, Cloud-Aerosol Lidar and Infrared Pathfinder Satellite Observations (CALIPSO) aerosol products within the first 1500 m of the vertical column (corresponding to the mean MBL depth over mid-latitude ocean (Rémillard et al., 2012)) are used, when available, to assess the predominant types of aerosol particles arriving at ENA during the events (Omar et al., 2009). CALIPSO classification includes six types of aerosol mixtures: clean continental, clean marine, dust, polluted continental, polluted dust, and smoke (Burton et al., 2013). Finally, post hoc analysis are performed using Tukey-

35 Kramer Honest Significant Different (HSD) test (Haynes, 2013) to determine whether there is significant difference between N_{tot}, size distribution, N_{CCN}, and CCN potential activation fraction (at SS 0.1% and 0.2%) means under unperturbed regional aerosol conditions and during the periods of time affected by long-range transported continental aerosols. The significance probability was assessed at the probability level of $p < 0.05$.

40 **3 Results and discussion**

The entrainment of continental particles from long-range transport represents a significant source of aerosols over mid-latitude oceans and have the potential of altering the regional aerosol regimes (Garrett and Hobbs, 1995; Honrath, 2004; Roberts et al., 2006; García et al., 2017; Zhang et al., 2017; Zheng et al., 2018). Here, we apply the algorithm to detect multiday transported aerosol events at ENA during the year 2017. Once the events have been identified, we first assess the aerosol seasonal regimes
5   at ENA under baseline conditions by removing the measurements affected by the arrival of continental aerosol plumes (Section 3.1). Subsequently, the multiday aerosol plume transport events are examined and categorized based on origin and composition and their impacts on aerosol physical properties, such as variation in particle number concentrations and shifts in size distribution, which affects the ability of particles to act as CCN era evaluated (Section 3.2).

10   **3.1 Regional aerosol regime under baseline conditions**

3.1.1 Concentration and size distribution of submicron aerosol particles

The concentration of submicron aerosol particles and their size distribution under baseline conditions at ENA show seasonal variations likely related to a combination of different regional emission sources and sink mechanisms. In remote marine regions like ENA, particles of marine origin, including sea spray aerosols and marine aerosols formed by biogenic volatile organic
15   compounds produced by marine phytoplankton, dominate the aerosol population in the marine boundary layer (Rinaldi et al., 2010; Lapina et al., 2011; Sanchez et al., 2018). Overall, we found lower concentrations of submicron particles in the winter and higher during late spring and summer (Fig. 1). Namely, the minimum monthly N_{tot} mean value was observed in January 2017 (260 ± 143 cm^{-3}), while the maximum monthly N_{tot} mean value was reached in June 2017 (523 ± 259 cm^{-3}), approximately two times the winter minimum. Our results are consistent with earlier studies and field campaigns conducted in the North
20   Atlantic ocean region which report low wintertime N_{tot} as the result of reduced contribution from ocean biological activities and higher occurrence of in-cloud precipitation and coalescence scavenging during winter months compared to the spring and summer (Pennypacker and Wood, 2017; Zheng et al., 2018; Quinn et al., 2019). Likewise, the concentration of particles in the Aitken and Accumulation modes follow similar seasonal trends with monthly mean minima in N_{At} and N_{Ac} in January 2017 ($N_{At} = 148 \pm 81$ cm^{-3}) and in November ($N_{Ac} = 90 \pm 53$ cm^{-3}) respectively, and maxima in June 2017 ($N_{At} = 360 \pm 97$ cm^{-3} N_{Ac}
25   $= 195 \pm 79$ cm^{-3}) (Fig. 1). Interestingly, we observed that summer mean N_{Ac} values, which are approximately doubled than in the winter, are significantly higher than the correspondent median N_{Ac} values (Fig. 1). The influence of local aerosol sources on Ac mode aerosols measurements at ENA is minimal and the data utilized here has been filtered to remove impact of potential local emissions (Gallo et al., 2020). However, in the summer, MBL baseline aerosol concentrations might be influenced by the entrainment of diluted and aged continental particles from the free troposphere which likely contributes to enhanced
30   concentration of particles in the Ac mode (Wang et al., 2021). This observation is consistent with previous studies investigating aerosol vertical profiles during the summer ACE-ENA field campaign (Wang et al., 2021), and over the Western North Atlantic during the NASA North Atlantic Aerosol and Marine Ecosystems Study campaign (NAAMES). Particles in the LA mode (not shown) showed the opposite seasonal trend reaching the maximum monthly mean value in the winter ($N_{LA} = 14 \pm 9$ cm^{-3} in January) and the lowest concentrations in the summer ($N_{LA} = 7 \pm 4$ cm^{-3} in August). However, throughout the entire year, the
35   total aerosol number concentration among the three particle modes is dominated by the At mode (yearly mean At mode contribution to $N_{tot} = 61\% \pm 3\%$) while the Ac mode is lower (yearly mean Ac mode contribution to $N_{tot} = 35\% \pm 4\%$) and LA mode represents only a small percentage of N_{tot} (yearly mean LA mode contribution to $N_{tot} = 3\% \pm 1\%$). Further analysis of the measured size distribution from the UHSAS instrument (measurement size range 70 - 1000 nm) during winter (January, February, November, and December 2017) and summer (May to September 2017) at ENA provide an insight into seasonal
40   variations of particle size. In the wintertime mean particle size D_p peaks at 128 nm (Fig. 2a), while in the summer mean mode D_p is shifts towards slightly larger sizes peaking at 147 nm (Fig. 2b). While the UHSAS lower size limit is at $D_p = 70$ nm, the

UHSAS size distribution measurements associated with the calculated N_{At}, and N_{Ac} and N_{La} suggest aerosol bimodal structure for both winter and summer. In the absence of the entrainment of particles of continental origins, the size distribution of particles in the MBL is shaped by different seasonal surface-ocean biogenic emissions, aerosol removal processes, and meteorological regimes (Behrenfeld et al., 2019). New particle formation events in the upper part of the decoupled MBL has been reported by previous studies and are due to a combination of reduced existing aerosol surface area, passage of cold fronts, reactive gas availability and high actinic fluxes (Bates et al., 1998; Kolstad et al., 2009; Zheng et al., 2021). At ENA, more frequent precipitation and drizzle in the winter lead to the removal of large particles, such as sea spray aerosols, and consequently low existing aerosol surface availability, which associated with wintertime cold temperature enhance the occurrence of new particles formation events. Once formed, the new particles grow into larger particles strongly contributing to the Aitken mode. The removal of At mode particles is largely driven by coagulation, while out-of-cloud condensation of At mode particles into Accumulation mode is weak due to DMS concentrations in the MBL (Zheng et al., 2018). While the condensational growth of Aitken mode aerosols only represent a minor source of Accumulation mode particles in the winter, enhanced wind speeds cause the production of sea spray aerosols at the ocean surface which significantly contribute to larger modes and explain the higher concentration of particles in the LA mode observed in January (Vignati et al., 2010; Zheng et al., 2018; Quinn et al., 2019). During late spring and summer, the phytoplankton bloom is responsible for strong ocean emissions of dimethylsulfide, whose oxidation products have been found to enhance the condensational growth of nucleation mode particles into the Aitken and subsequently to the Accumulation modes (O'Dowd et al., 1997; Andreae et al., 2003; Zheng et al., 2018). Furthermore, photochemistry and/or oxidation of oxygenated gas-phase organic compounds produce secondary organic aerosols at the surface layer which contribute to the growth of Aitken mode particles during late summer when phytoplankton activity is lower (Mungall et al., 2017).

3.1.2 CCN concentrations and potential activation fraction

The concentration of CCN in the remote marine boundary layer is dominated by ocean-derived particles. Previous studies have reported that the major sources of CCN over the Atlantic Ocean include sea salt aerosols enriched in organics and marine biogenic gases that oxidize and condense onto existing particles (Charlson et al., 1987; Pandis et al., 1994; O'Dowd et al., 2004; Yoon et al., 2007; Korhonen et al., 2008; Quinn and Bates, 2011; Sanchez et al., 2018; Zheng et al., 2018). Here, we assess the seasonal variations of CCN concentrations (N_{CCN}) at ENA under baseline conditions, and we investigate the CCN potential activation fractions to evaluate how the different aerosol seasonal regimes affect the ability of the particles to act as CCN.

Throughout the year 2017, mean monthly CCN concentration values were low, as expected for clean marine environments (Ovadnevaite et al., 2014) and seasonal variations are noticeable at both super-saturations (Fig. 3). Lower monthly mean N_{CCN} values were reported in the winter and spring (minimum in December 2017 and $N_{CCN,0.1\%}$ = 69 ± 27 cm⁻³ at SS of 0.1 and $N_{CCN,0.2\%}$ = 108 ± 38 cm⁻³ cm⁻³ at SS 0.2%) while monthly N_{CCN} mean values were higher in the summer (maximum monthly N_{CCN} mean values in July 2017 and = 141 ± 53 cm⁻³ at SS of 0.1 and = 178 ± 68 cm⁻³ at SS 0.2%). The CCN potential activation fraction follows a different seasonal trend exhibiting higher values in late summer/fall and winter (mean AF SS 0.1% = 0.27 ± 0.03, and mean AF SS 0.1% = 0.41 ± 0.02) and lower in the spring (mean AF SS 0.1% = 0.22 ± 0.01, and mean AF SS 0.1% = 0.32 ± 0.04). As observed in the previous section, reduced ocean biological activity in the winter leads to low number particle concentration and consequently to low concentrations of cloud condensation nuclei in the MBL. Furthermore, CCN removal through in-cloud coalescence scavenging processes associated with high occurrence of precipitation events in the winter and spring might also play a role in constraining CCN concentrations (Sharon et al., 2006; Zheng et al., 2018). However, the higher CCN potential activation fraction in wintertime than in the spring indicates that winter aerosol particles have a more elevated ability to act as cloud condensation nuclei. A slightly lower ratio of N_{Ac} to N_{tot} in the winter than in the summer (mean Ac mode ratio to N_{tot} = 31% and 37% respectively in the winter and in the summer) suggest that particle compositions play an important

role in CCN formation at ENA. Consistent with our observations, earlier studies have pointed out that wind-generated sea spray aerosols enriched by particulate organic matter and biogenic sulfate, as observed at ENA in the winter are a stronger source of CCN than phytoplankton-derived aerosols (Quinn and Bates, 2011; Sanchez et al., 2018; O'Dowd et al., 2004). Summertime high N_{CCN} and CCN potential activation fraction are to a large degree related to a combination of fast

5   condensational growth, reduced wet scavenging and elevated sulfate ocean emissions caused by the final phase of the phytoplankton bloom and microbial activities (Saliba et al., 2020).

3.2 Multiday transported aerosol plume events at ENA in 2017

We apply the algorithm for detecting multiday aerosol plume transport events at ENA to the in-situ aerosol measurements

10   collected at ENA ARM during 2017. We identify 9 events affecting ENA through the entire year. The duration of the events was typically greater than 2 days with an average time period of 3 days, and total duration of 642 hours corresponding to ~7.5% of the year. A summary of the events, including duration, origins, aerosol CALIPSO classification and values of the three aerosol properties used to identify the events (median number concentration of D_p 100-1000 nm particles, mean single scattering albedo of submicron particles at λ 464 nm, and mean black carbon concentration) is shown in Table 2.

15   The origin of the air masses arriving at ENA and their paths, assessed by performing 10-day Hysplit backward trajectories, indicate a seasonal pattern likely controlled by seasonal meteorological regimes and atmospheric circulation in the Northern Hemisphere (Zhao et al., 2012). A number of studies reported Sahara dust intrusions into the North Atlantic MBL in the late fall and winter associated with cyclonic dust-storms in the North Africa region (Nakamae and Shiotani, 2013; Choobari et al., 2014; Laken et al., 2014; Logan et al., 2014; Cuevas et al., 2017). In accordance with these observations, we found two events

20   of southward transport from northern African and Portuguese flows to ENA in the months of November and December 2017, likely favoured by Artic anticyclone, polar vortex, and midlatitude circulation. A large fraction of air masses arriving at ENA throughout the year are attributed to transport from industrialized continental areas as North Europe, Canada, and North America due to midlatitudes cyclones and convection (García et al., 2017). Continental aerosol particles are emitted in the boundary layer by anthropogenic processes and are subsequently transported for several days within the free troposphere before

25   entrainment into the marine boundary layer over the North Atlantic ocean (Honrath, 2004; Wood et al., 2015; Cavalli et al., 2016). Here, we observed two aerosol transport events with Northern European origins in the months of January and April 2017. We also identified aerosol transports events from North America and Canada between May and September 2017. Our results are consistent with previous studies conducted in the North Atlantic region which reported dominant eastward direction from North America in the late spring and summers (Zhao et al., 2012) and high aerosol loading due to pollution outflow and

30   biomass burning emissions (Honrath et al., 2004; Alves et al., 2007; Dzepina et al., 2015; García et al., 2017; Zheng et al., 2020; Wang et al., 2021b).

Analysis of CALIPSO aerosol products provide further insights on the type of aerosols transported. Consistent with the origin of the emission sources we observe dust and marine aerosol mixtures associated with transport from the Artic and Canada in March 2017, and from North Africa in November and December 2017, while the airflows originating from industrialized areas

35   (January, April, May, and October 2017) typically consisted of a mixture of polluted continental aerosol, smoke, and marine particles. Simultaneously, NASA Worldview VIRS 375 observations of the multiday aerosol plume transport events occurring in August and September 2017 show elevated concentration of smoke over ENA due to a particularly intense wildfire season in North America and Canada, and therefore suggesting the presence of biomass burning aerosols as also previously observed by Zheng et al., 2020.

40   In the following three sections, we discuss specific case studies representatives of the diverse continental plumes arriving at ENA through the year. Furthermore, in section 3.2.4, Table 3, and Fig. 8, we provide a summary statistic of the of the influence of continental aerosol emissions on aerosol population and CCN concentrations at ENA.

3.2.1 Multiday transport event of dust and marine mixture aerosols from North Africa

The transport of air masses from North Africa to the North Atlantic ocean region during the winter is the result of the shift of the subtropical high pressure system south-eastward, and enhancing trade winds over the Sahara (Chiapello, 2005; Riemer et al., 2006; Alonso-Perez et al., 2011; Nakamae and Shiotani, 2013). Sahara dust intrusions in North Atlantic MBL have been

5   reported by a number of studies (Choobari et al., 2014; Laken et al., 2014; Cuevas et al., 2017) especially between January and March (Alonso-Pérez et al., 2007). In this study, we identified the arrival of air masses from Western Sahara and Mauritania to ENA between December 7th and December 12th, 2017 (Fig. 4). Here, we assess CALIPSO retrievals, aerosol hygroscopicity parameters as a function of dry particle size (κ_{HTDMA}), and concentrations of black carbon and CO to confirm the nature of the aerosol particles arriving at ENA during the event (Fig. 7a-d). CALIPSO aerosol profiles indicate a mixture of dust and marine

10   aerosol in the marine boundary layer. Simultaneously, κ_{HTDMA} values were = 0.22, 0.30, 0.37, 0.322, 0.37 respectively for dry particles with D_p = 50, 100, 150, 200, and 250 nm (Fig. 7a). For representative atmospheric aerosol particles, the hygroscopicity parameter κ_{HTDMA} ranges from 0 to 1.4 where high values (> 0.5) indicate very hygroscopic inorganic species such as sodium chloride, and low values indicate non-hygroscopic organic enriched compounds (0.01 < κ_{HTDMA} < 0.5 slightly to very hygroscopic, and κ_{HTDMA} < 0.01 non-hygroscopic components) (Petters and Kreidenweis, 2007). The κ_{HTDMA} values observed

15   here suggest the potential presence of insoluble minerals such as Saharan dust mixed to slightly hygroscopic organic enriched compounds of marine origins (Koehler et al., 2009; Zhang et al., 2014). Mean black carbon concentrations during the event were higher than for the rest of the month (event mean BC = 101 ± 17 ng m^{-3} and up to 120 ng m^{-3} against baseline mean BC in December 2017 = 26 ± 8 ng m^{-3}), while CO levels remain constant (event mean CO = 101.4 ± 3 ppmv against baseline mean CO in December 2017 = 100.9 ± 9 ppmv). Consistent with our results, previous studies found that aerosol from biomass

20   burning activities occurring during the dry season in the Sahel region (Boreal winter) can mix with the dust affecting the composition of the particles without transport of smoke over the Atlantic (Ben-Ami et al., 2009; Redemann et al., 2021). The arrival of the aerosol plume at ENA was associated with an increase in mean submicron aerosol number concentration approximately doubled that under than under baseline conditions (mean event N_{tot} = 683 ± 135 cm^{-3} compared to monthly mean N_{tot} December 2017 = 313 ± 128 cm^{-3}). Aitken and Accumulation mode particle concentrations both double, while the

25   relative contributions of the two modes to N_{tot} remained similar to baseline with mean At contribution = 59% and mean Ac contribution = 38% of N_{tot} (N_{At} / N_{Ac} change = 0.3%) (Fig. 7b), indicating that the particles arriving at ENA during the event had a size distribution similar to that of the regional aerosol. The peak of the size distribution in the Accumulation mode was at 127 nm for both event and baseline aerosol regimes, while the concentration of D_p > 200 nm particles was only 11% of N_{Ac}. The evolution of the size distribution of dusty aerosols during transport over the North Atlantic has been the focus of previous

30   studies that report loss of coarse mode particles due to gravitational settling and wet deposition just off the coast of Africa, while finer particles remain in suspension and can be transported for longer distances (Maring, 2003; Kalashnikova and Kahn, 2008; Lawrence and Neff, 2009; Mahowald et al., 2014; Friese et al., 2016). The concentration of CCN increased during the event following a similar trend of N_{tot} (mean event N_{CCN} = 70 ± 27 cm^{-3} and 109 ± 31 cm^{-3} compared to monthly mean N_{CCN} December 2017 = 165 ± 32 cm^{-3} and 280 ± 36 cm^{-3} respectively for SS 0.1% and 0.2%, and corresponding increases by factors

35   of 2.3 and 2.5 respectively over baseline value observed during the month of December 2017) leading to almost no change in CCN potential activation fraction (event AF = 0.25 and 0.42 compared to AF in December 2017 = 0.26 and 0.42 respectively for SS 0.1% and 0.2%). Furthermore, the linear regression between N_{tot} and N_{CCN} during the event and under baseline conditions show similar slopes (at SS 0.1%: N_{CCN} = 0.23N_{tot}, and N_{CCN} = 0.18N_{tot} respectively during the event and under baseline conditions at SS 0.2%: N_{CCN} = 0.40N_{tot} and N_{CCN} = 0.30N_{tot} during the event and under baseline conditions respectively),

40   indicating that that the enhanced concentration of CCN observed during the event, is mainly due to higher N_{tot} (Fig. 7c). When comparing the potential activation fraction to the ratio of N_{Ac} and N_{At} we observed a good linear regression (AF= 0.42N_{Ac}/N_{At},

with r^2 =0.93 at SS 0.1%, and AF= $0.67N_{Ac}/N_{At}$, with r^2 =0.90 at SS 0.2%) suggesting a strong correlation between CCN activated and particle size (Fig. 7d).

3.2.2 Multiday transport event of polluted continental and marine mixture aerosols from North Europe

5   Air masses from the Artic and Europe occasionally reach the North East Atlantic during the spring months (Zheng et al., 2018), while transport from this region during summer and winter is rare (Zhang et al., 2017). Here, we describe a transport event of marine and polluted continental aerosol mixture at ENA which occurred between April 20th and April 22nd, 2017. The aerosol plume originated from the Artic and before entraining into the MBL at ENA, travelled for several days over Northern Europe (Fig. 5). CALIPSO aerosol retrievals indicate the presence of a mixture of marine and polluted continental aerosols (Table 2).

10 Typically, during the transport to ENA, air masses are contaminated by industrial and urban pollution over industrialized European regions. Observational studies have pointed out that a major contribution to aerosol emissions in Central and Northern Europe is by particles from solid fuel combustion with both residential and urban/industrial origins (Chirico et al., 2010; Fuller et al., 2013; Lin et al., 2018), while biomass burning from wild-fires (Pio et al., 2008) and agricultural fires only contribute marginally in eastern Europe (Stohl et al., 2007). As a result, BC, primary organic aerosols, and VOC are emitted

15 in the atmosphere by incomplete combustion processes. These particles show no significant hygroscopic growth, however once in the atmosphere, photochemical aging processes and changes in mixing state (e.g. coating of hydrophilic material) significantly increase the hygroscopicity of the particles (Weingartner et al., 1995; Wang et al., 2010) and their ability to act as CCN (Wittbom et al., 2014). Here, we observed κ_{HTDMA} values almost constant across the measured particle size range of 50 to 250 nm (κ_{HTDMA} values = 0.44, 0.44, 0.49, 0.48, 0.49 respectively for dry particles with D_p = 50, 100, 150, 200, and 250

20 nm) which suggest the presence of aged, well-mixed particles likely dominated by sulphate and organic compounds (Petters and Kreidenweis, 2007) (Fig. 7e). Furthermore, mean BC concentration = 121 ± 33 ng m^{-3} and up to 176 ng m^{-3} during the time period affected by the transport of particles from Northern Europe, and higher than what was observed during baseline conditions (monthly mean in April 2017 = 36 ± 16 cm^{-3} ng m^{-3}) also confirmed the presence of particles with urban and industrial origins. CO levels were also slightly higher than under baseline conditions ranging between 120 and 135 ppb

25 (baseline CO concentration < 112 ppb) indicative of moderately polluted boundary layer (Spackman et al., 2008). Statistically significant increase in N_{tot} was observed during the event (mean N_{tot} event = 804 ± 155 cm^{-3} against monthly mean N_{tot} April 2017 = 414 ± 124 cm^{-3}). The Ac mode particle concentration was by 3-fold higher during the event with the size distribution peaking between 135 and 140 nm, while the increase in N_{At} was significantly lower (= +25%) (Fig. 7e,f). Consequently, the mean particle diameter shifted toward larger sizes and the contribution of the Accumulation mode to N_{tot} became predominant

30 over the Aitken mode (At contribution = 40 %, Ac contribution = 57% corresponding to change in N_{At} / N_{Ac} = 148%). During the event, N_{CCN} exhibited mean values of 179 ± 45 cm^{-3} at SS 0.1% (compared to monthly mean April 2017 = 84 ± 37 cm^{-3}), and 379 ± 23 cm^{-3} at SS 0.2% (compared to monthly mean April 2017 = 122 ± 67 cm^{-3}). The total CCN active fraction was also significant higher during the event being 30% at SS 0.1%, and = 49% at SS 0.2%, and corresponding to 34% and 53% increase at SS 0.1% and SS 0.2% respectively. The prevalence of moderately hygroscopic particles in the accumulation mode

35 were likely responsible for the higher CCN-activation fractions observed during the period affected by the entrainment of long-range transported aerosols. The slopes of the linear regression between N_{tot} and N_{CCN} are higher during the event than under baseline conditions (at SS 0.1%: N_{CCN} = $0.28N_{tot}$ and N_{CCN} = $0.19N_{tot}$ respectively during the event and under baseline conditions, and at SS 0.2%: N_{CCN} = $0.46N_{tot}$ and N_{CCN} = $0.28N_{tot}$ during the event and under baseline conditions respectively) indicating the enhanced ability of the continental transported particles to act as CCN (Fig. 7g). Thus, increase in N_{CCN} during

40 the event were likely trigged by the combination of high N_{tot}, elevated relative contribution of Ac mode particles to N_{tot}, and high κ_{HTDMA} values. These observations are supported by the shape of the curves generated comparing the potential activation fraction to the ratio of N_{Ac} and N_{At} (Fig. 7h). The linear regression at SS 0.1% (AF= $0.17 + 0.07N_{Ac}/N_{At}$, with r^2 =0.83) versus

the lognormal distribution observed at SS 0.2% indicate that, while at lower supersaturation the number of activated particles was mainly driven by a shift towards larger particle size, at higher supersaturation particle composition also played a strong role.

3.2.3 Multiday transport event of biomass burning aerosols from North America

Pollution and biomass burning aerosols from North America commonly impact the remote North Atlantic region (Honrath, 2004; Alves et al., 2007; Dzepina et al., 2015; García et al., 2017). Zhang et al. (2017) reported that the 16%, 15%, and 13% of the air masses intercepted at Pico Mountain respectively in spring, summer and fall are influenced by North America anthropogenic sources with the 7.3% being associated with wildfire influences. Namely, during summer 2017, several severe wildfires raged in United States and northwest Canada (Kloss et al., 2019). Biomass burning particles in the smoke from the wildfires are typically released and into the lower extratropical stratosphere and transported by cold fronts through the jet stream eastward over the Atlantic Ocean where cold descending airstreams favour their entrainment in the MBL (Owen et al., 2006; Khaykin et al., 2018; Peterson et al., 2018).Here we present a detailed characterization of a long-range transport event of biomass burning aerosols that affected ENA between September 09th and September 13th, 2017. During the period in analysis, the arrival of air masses from North America are associated with elevated number of active wildfires in North America and Canada as observed by NASA Worldview VIIRS 375 active fires counts between September 1st and September 15th, 2017. (Fig. 6). Long-range transported biomass burning aerosols from North American and Canadian wildfires at ENA in August 2017 have been also reported by a previous study (Zheng et al., 2020). Aerosol optical properties and aerosol hygroscopicity parameters confirm the presence of biomass burning particles. Namely, mean aerosol absorption coefficients at λ 648 nm = 1.04 ± 0.28 Mm^{-1} and mean SSA at λ 464 = 0.93 ± 0.02 are in agreement with values reported by previous studies of North American aged wildfire aerosols (Clarke et al., 2007; Zheng et al., 2020). Furthermore, κ_{HTDMA} values were lower than under baseline conditions at 0.32, 0.31, 0.28, 0.28, 0.29 for particles with D_p = 50, 100, 150, 200, and 250 respectively,(Fig. 7i) likely due to high concentration of organics (total organics up to 8.65 μg m^{-3}, Aerosol Chemical Speciation Monitor data not shown) as reported by earlier laboratories studies on aged biomass fuel representative of North American wildfires (Petters et al., 2009; Lathem et al., 2013) (Fig. 7i). The event did not cause a significant increase in particle number concentrations (mean event N_{tot} = 530 ± 189 cm^{-3} compared to monthly mean N_{tot} December 2017 = 421 ± 139 cm^{-3}) which were dominated by particles with D_p > 100 nm (mean At and Ac contributions to N_{tot} = 37% and 58% respectively) (fig. 7j). Fresh biomass burning aerosol commonly has an unimodal distribution with D_p between 30 and 100 nm (Hosseini et al., 2010; Levin et al., 2010). However, during the transport events, aerosol processes such as coagulation and condensation of organic material onto existing particles lead to the formation of larger particles with D_p between 170 and 300 nm and to narrower size distribution compared to that of freshly emitted particles (Zellner, 2000; Dentener et al., 2006; Janhäll et al., 2010). Consequently, these aerosol particles are more effective as CCN as suggested by the CCN potential activation fraction values = 0.44 and 0.70 at SS 0.1% and 70% at SS at 0.2%. These potential activation fractions are approximately twice the values found under baseline conditions. Similarly, the r^2 and slopes obtained through linear regression between N_{tot} and N_{CCN} are higher under periods affected by the events compared to baseline conditions (r^2 = 0.56 with a slope of 0.44 ± 0.005 at SS 0.1% and r^2 = 0.66 with a slope of 0.68 ± 0.007 at SS 0.2% during the event, against r^2 = 0.32 with a slope of 0.22 ± 0.001 at SS 0.1% and r^2 = 0.40 with a slope of 0.34 ± 0.007 at SS 0.2%) (Fig. 7k). The CCN concentration was 220% and 227% higher respectively at SS 0.1% and SS 0.2% during the event then for rest of the month of September 2017. Furthermore, comparing the potential activation fraction to the ratio of N_{Ac} and N_{At} we obtained lognormal distributions at both SS 0.1% and SS 0.2% indicating that particle composition also affect the concentration of particles that can act as CCN (Fig. 7l). These results demonstrate that aged wildfire aerosols dominated by accumulation mode particles have a strong ability to act as CCN and affect CCN budget at ENA with potential effects on Earth's albedo, clouds lifetime and precipitation (Albrecht, 1989).

3.2.4 Continental aerosol influences on regional aerosols properties and CCN

Multiday aerosol plume transport events at ENA influence regional aerosol properties and CCN concentrations. However, the extent of changes in N_{tot} and particle size mode are dependent on the origin and composition of the transported particles and

5 affects CCN concentrations differently. To assess the correlation between origin and composition of the multiday transport events and their influence on baseline aerosol properties at ENA, we perform post hoc Tukey-Kramer HSD analysis determining whether the arrival of the continental aerosol plumes produced statistically significant changes on a) baseline aerosol number concentrations, b) aerosol mode sizes in terms of relative Aitken and Accumulation modes contributions to N_{tot} (expressed as the ratio between N_{At} and N_{Ac} (N_{At} / N_{Ac})), and c) CCN potential activation fraction (Table 3).

10 The arrival of mixture of dust and marine aerosol plumes as observed in the month of March 2017 with Artic and Canada origins, and in November and December 2017 from North Africa, cause statistically significant increase in N_{tot} (123%), accompanied by statistically non-significant shifts in size distribution and CCN potential activation fraction (Fig 8a). Namely, particle concentrations in the At and Ac mode show comparable increase (mean increase = 117% and 146% respectively for N_{At} and N_{Ac}) (Fig. 8a), and consequently the relative Aitken and Accumulation mode contributions to N_{tot} remain almost

15 constant (N_{At} / N_{Ac} changes < 1%), with the mean At and Ac modes being respectively 59% and 38% of the total number concentration (Fig. 8b) and similar to the baseline condition (where At mode contributes 61% and Ac mode 36% to N_{tot}) (Fig. 8b). The gravitational settling of coarse particle during the transport to ENA is likely the reason why we did not find significant shifts towards larger particle sizes (Lawrence and Neff, 2009; Mahowald et al., 2014; Friese et al., 2016). The arrival of the aerosol plumes at ENA also lead to higher CCN concentrations (mean increase = 122% and 162% respectively at SS 0.1% and

20 SS 0.2%) than under unperturbed aerosol regime. However, these increases were not accompanied by statistically significant changes in CCN potential activation fractions which remained similar to the baseline conditions during the entire duration of the event (mean AF during the event: $AF_{0.1\%}$ = 0.26 and $AF_{0.2\%}$ = 0.42 against mean AF under unperturbed aerosol conditions: $AF_{0.1\%}$ = 0.27 and $AF_{0.2\%}$ = 0.41) (Fig. 8a). These results indicate that mixture of dust and marine aerosol particles have the same ability of acting as CCN that marine regional aerosol at ENA have, and the elevated N_{CCN} are a consequence of increased

25 N_{tot}.

The multiday aerosol plume transport events that occurred in January, April, May, and October of 2017, dominated by a mixture of marine and polluted continental aerosol and originated in continental industrialized areas such as Northern Europe, and North America, caused significant changes in submicron particle number concentration, size distribution, and CCN potential activation fraction. Furthermore, we found ~ 4-fold higher aerosol absorption coefficient at 648 nm and mean

30 absorption Angstrom exponent at λ 460/648 nm =1.04 ± 0.1 Mm^{-1} during the events, and mean black carbon concentration was = 177 ± 76 ng m^{-3} and up to 319 ng m^{-3} against mean concentration under unperturbed aerosol conditions of 35 ± 16 ng m^{-3} (data not shown), as expected for aerosol with enhanced contribution from fossil fuel and urban pollution sources (Clarke et al., 2007; Cazorla et al., 2013). During the events, the number concentration of submicron particles at ENA experienced a mean increase of 108% due to 37% and 256% mean increases respectively in the N_{At} and N_{Ac} modes (and corresponding to N_{At}

35 / N_{Ac} changes > 200%) (Fig. 8a). Therefore, the Accumulation mode became predominant over the Aitken mode. Namely, during multiday aerosol plume transport events the average contributions of the At mode to the total number particle concentrations was 42% (between 35% and 45% depending on the event), while the average contributions of the Ac mode to N_{tot} was 56% (between 45% and 60%) (Fig. 8b). The aforementioned changes in aerosol concentrations and shifts in size distributions caused higher CCN concentrations (mean increase = 176% and 240% respectively at SS 0.1% and SS 0.2%) and

40 statistically significant increases in CCN potential activation fractions (mean AF during the event: $AF_{0.1\%}$ = 0.34 and $AF_{0.2\%}$ = 0.55 corresponding to AF increases between 25% and 50%) (Fig. 8a). This result suggests that polluted particles of continental

origins with D_p > 100 nm are sufficiently large to readily serve as CCN, and have the potential to substantially increase CCN concentrations in marine remote regions (Hudson and Xie, 1999).

Finally, the long-range transport of smoke and biomass burning aerosols identified in months of August and September 2017 did not impact the concentration of submicron aerosol particles, but did cause statistically significant shifts in particle size

5   distribution and an increase in the CCN potential activation fraction. These events caused only a weak increase (< +25%) in submicron number particle concentrations accompanied by the decrease of Aitken mode particle concentrations (mean reduction = -39% and down to -50%) and increase of Accumulation mode particle concentrations (mean increase = +115%) (Fig. 6i, j). Thus, during the High CCN activation events, At mode particles only represented 33% of Ntot, while mean Ac mode contribution to N_{tot} was = 63% (Fig. 8b). The shift in size distribution corresponded to a decrease in the N_{At}/N_{Ac} ratio of

10 ~300%. Simultaneously, mean CCN concentrations and AF values were 118% and 119% higher during the event compared to baseline conditions at SS of 0.1% and 0.2% respectively, and associated with elevated mean CCN potential activation fraction (= 0.46 at SS 0.1%, and 0.74 at SS 0.2) (Fig. 8a). These findings suggest that the shape of the submicron particle size distribution exerts a significant effect on the ability of aerosol to act as CCN, and the arrival of biomass burning aerosols from continental wildfires significantly affects the CCN concentrations at ENA.

4. Conclusions

Multiday aerosol events due to long-range transport of continental aerosols, are observed at ENA throughout the year. In this study we develop an algorithm that integrates submicron aerosol size distribution, single scattering albedo and black carbon

20 concentration measurements to identify multiday aerosol plume transport events occurring at ENA in 2017. In the year 2017, we identified nine events of long-range transported particles (with durations >24 hours), corresponding to ~7.5% of the year. Analysis of 10-day HYSPLIT backward trajectories and CALIPSO aerosol products indicate different origins and aerosol compositions of the air masses arriving at ENA during the transport events. Namely, we observe the arrival of 1) mixture of dust and marine aerosols from the Artic and Canada in March 2017, and from North Africa in November and December 2017,

25 2) mixture of marine and polluted continental aerosols from Northern Europe and North America in January, April, May, and October 2017, and 3) pollution and biomass burning aerosol form North America and Canada in the months of August and September 2017. Subsequently, we assess the influence of the aerosol plumes composition on CCN concentrations at ENA, investigating the mechanisms that trigger the increase in N_{CCN}. The events characterized by the arrival of mixture of dust and marine aerosols at ENA causeed statistically significant increases in N_{tot}, while the aerosol size distribution and CCN potential

30 activation fraction remained similar to baseline conditions, indicating that greater N_{CCN} were attributable to the elevated concentration of particles during the event. Mixture of marine and polluted continental aerosol plumes showed high CCN concentrations attributable to both high N_{tot}, and predominance of large particles (D_p > 100 nm) of sufficient size to readily serve as CCN. Conversely, despite only causing slight increases in N_{tot}, the events dominated by the arrival of biomass burning aerosols were characterized by the presence of particles with strong ability to act as CCN leading to two-fold higher N_{CCN}.

35 Based on our analysis, in 2017, the transport of continental particles at ENA, caused a total N_{CCN} increase by ~22%, impacting ~28 days, and strongly contributing to the CCN concentrations at ENA. Namely, we observed that plumes dominated by mixture of dust and marine aerosols, mixture of marine and polluted continental aerosols, and biomass burning aerosols can cause respectively 6.5%, 8%, and 7.4% increase in N_{CCN}. Furthermore, we showed that, once the multiday aerosol event is identified, the analysis of changes in baseline N_{tot} and particle size distribution as well as their correlation, might be used as

40 proxy to estimate how CCN is affected. Based on the characteristics of the type events discussed above, the development of an algorithm to predict N_{CCN} variations during multiday events of long-range transport of aerosols and their influence on CCN concentrations at ENA might be explored in the future.

Data availability: data were obtained from the Atmospheric Radiation Measurement (ARM) User Facility, a U.S. Department of Energy Office of Science user facility sponsored by the Office of Biological and Environmental Research (available at

5   https://www.archive.arm.gov/discovery).

Competing interest: The authors declare that they have no conflicts of interest.

Acknowledgements: The work was supported by the Atmospheric Radiation Measurement (ARM) program, funded by the U.S. Department of Energy (DOE), Office of Science, Office of Biological and Environmental Research. We acknowledge the

10   ARM Research Facility, a user facility of the U.S. DOE, Office of Science, sponsored by the Office of Biological and Environmental Research for providing data. Robert Wood acknowledges funding from ASR award DE-SC0021103. We acknowledge the use of data and/or imagery from NASA's Fire Information for Resource Management System (FIRMS) (https://earthdata.nasa.gov/firms), part of NASA's Earth Observing System Data and Information System (EOSDIS).

We also acknowledge the ENA ARM Site Operators, Carlos Sousa, Tercio Silva and Bruno Cunha.

References

Albrecht, B. A.: Aerosols, Cloud Microphysics, and Fractional Cloudiness, Science, 245, 1227–1230, https://doi.org/10.1126/science.245.4923.1227, 1989.

5 Albrecht, B. A., Bretherton, C. S., Johnson, D., Scubert, W. H., and Frisch, A. S.: The Atlantic Stratocumulus Transition Experiment—ASTEX, Bull. Am. Meteorol. Soc., 76, 889–904, https://doi.org/10.1175/1520-0477(1995)076<0889:TASTE>2.0.CO;2, 1995.

Alonso-Pérez, S., Cuevas, E., Querol, X., Viana, M., and Guerra, J. C.: Impact of the Saharan dust outbreaks on the ambient levels of total suspended particles (TSP) in the marine boundary layer (MBL) of the Subtropical Eastern North Atlantic Ocean, Atmos. Environ., 41, 9468–9480, https://doi.org/10.1016/j.atmosenv.2007.08.049, 2007.

10 Alonso-Perez, S., Cuevas, E., Perez, C., Querol, X., Baldasano, J. M., Draxler, R., and De Bustos, J. J.: Trend changes of African airmass intrusions in the marine boundary layer over the subtropical Eastern North Atlantic region in winter: TREND CHANGES OF AFRICAN AIRMASS INTRUSIONS, Tellus B, 63, 255–265, https://doi.org/10.1111/j.1600-0889.2010.00524.x, 2011.

Alves, C., Oliveira, T., Pio, C., Silvestre, A. J. D., Fialho, P., Barata, F., and Legrand, M.: Characterisation of carbonaceous 15 aerosols from the Azorean Island of Terceira, Atmos. Environ., 41, 1359–1373, https://doi.org/10.1016/j.atmosenv.2006.10.022, 2007.

Andreae, M. O., Andreae, T. W., Meyerdierks, D., and Thiel, C.: Marine sulfur cycling and the atmospheric aerosol over the springtime North Atlantic, Chemosphere, 52, 1321–1343, https://doi.org/10.1016/S0045-6535(03)00366-7, 2003.

Bates, T. S., Kapustin, V. N., Quinn, P. K., Covert, D. S., Coffman, D. J., Mari, C., Durkee, P. A., De Bruyn, W. J., and 20 Saltzman, E. S.: Processes controlling the distribution of aerosol particles in the lower marine boundary layer during the First Aerosol Characterization Experiment (ACE 1), J. Geophys. Res. Atmospheres, 103, 16369–16383, https://doi.org/10.1029/97JD03720, 1998.

Behrenfeld, M. J., Moore, R. H., Hostetler, C. A., Graff, J., Gaube, P., Russell, L. M., Chen, G., Doney, S. C., Giovannoni, S., Liu, H., Proctor, C., Bolaños, L. M., Baetge, N., Davie-Martin, C., Westberry, T. K., Bates, T. S., Bell, T. G., Bidle, K. D., 25 Boss, E. S., Brooks, S. D., Cairns, B., Carlson, C., Halsey, K., Harvey, E. L., Hu, C., Karp-Boss, L., Kleb, M., Menden-Deuer, S., Morison, F., Quinn, P. K., Scarino, A. J., Anderson, B., Chowdhary, J., Crosbie, E., Ferrare, R., Hair, J. W., Hu, Y., Janz, S., Redemann, J., Saltzman, E., Shook, M., Siegel, D. A., Wisthaler, A., Martin, M. Y., and Ziemba, L.: The North Atlantic Aerosol and Marine Ecosystem Study (NAAMES): Science Motive and Mission Overview, Front. Mar. Sci., 6, 122, https://doi.org/10.3389/fmars.2019.00122, 2019.

30 Ben-Ami, Y., Koren, I., and Altaratz, O.: Patterns of North African dust transport over the Atlantic: winter vs. summer, based on CALIPSO first year data, Atmospheric Chem. Phys., 9, 7867–7875, https://doi.org/10.5194/acp-9-7867-2009, 2009.

Bond, T. C. and Bergstrom, R. W.: Light Absorption by Carbonaceous Particles: An Investigative Review, Aerosol Sci. Technol., 40, 27–67, https://doi.org/10.1080/02786820500421521, 2006.

Bond, T. C., Anderson, T. L., and Campbell, D.: Calibration and Intercomparison of Filter-Based Measurements of Visible 35 Light Absorption by Aerosols, Aerosol Sci. Technol., 30, 582–600, https://doi.org/10.1080/027868299304435, 1999.

Bony, S.: Marine boundary layer clouds at the heart of tropical cloud feedback uncertainties in climate models, Geophys. Res. Lett., 32, L20806, https://doi.org/10.1029/2005GL023851, 2005.

Bullard, R. L., Kuang, C., Uin, J., Smith, S., and Springston, S. R.: Aerosol Inlet Characterization Experiment Report, https://doi.org/10.2172/1355300, 2017.

40 Burton, S. P., Ferrare, R. A., Vaughan, M. A., Omar, A. H., Rogers, R. R., Hostetler, C. A., and Hair, J. W.: Aerosol classification from airborne HSRL and comparisons with the CALIPSO vertical feature mask, Atmospheric Meas. Tech., 6, 1397–1412, https://doi.org/10.5194/amt-6-1397-2013, 2013.

Carslaw, K. S., Lee, L. A., Reddington, C. L., Pringle, K. J., Rap, A., Forster, P. M., Mann, G. W., Spracklen, D. V., Woodhouse, M. T., Regayre, L. A., and Pierce, J. R.: Large contribution of natural aerosols to uncertainty in indirect forcing, 45 Nature, 503, 67–71, https://doi.org/10.1038/nature12674, 2013.

Cavalli, F., Alastuey, A., Areskoug, H., Ceburnis, D., Čech, J., Genberg, J., Harrison, R. M., Jaffrezo, J. L., Kiss, G., Laj, P., Mihalopoulos, N., Perez, N., Quincey, P., Schwarz, J., Sellegri, K., Spindler, G., Swietlicki, E., Theodosi, C., Yttri, K. E., Aas,

W., and Putaud, J. P.: A European aerosol phenomenology -4: Harmonized concentrations of carbonaceous aerosol at 10 regional background sites across Europe, Atmos. Environ., 144, 133–145, https://doi.org/10.1016/j.atmosenv.2016.07.050, 2016.

Cazorla, A., Bahadur, R., Suski, K. J., Cahill, J. F., Chand, D., Schmid, B., Ramanathan, V., and Prather, K. A.: Relating aerosol absorption due to soot, organic carbon, and dust to emission sources determined from in-situ chemical measurements, Atmospheric Chem. Phys., 13, 9337–9350, https://doi.org/10.5194/acp-13-9337-2013, 2013.

Charlson, R. J., Lovelock, J. E., Andreae, M. O., and Warren, S. G.: Oceanic phytoplankton, atmospheric sulphur, cloud albedo and climate, Nature, 326, 655–661, https://doi.org/10.1038/326655a0, 1987.

Chiapello, I.: Understanding the long-term variability of African dust transport across the Atlantic as recorded in both Barbados surface concentrations and large-scale Total Ozone Mapping Spectrometer (TOMS) optical thickness, J. Geophys. Res., 110, D18S10, https://doi.org/10.1029/2004JD005132, 2005.

China, S., Scarnato, B., Owen, R. C., Zhang, B., Ampadu, M. T., Kumar, S., Dzepina, K., Dziobak, M. P., Fialho, P., Perlinger, J. A., Hueber, J., Helmig, D., Mazzoleni, L. R., and Mazzoleni, C.: Morphology and mixing state of aged soot particles at a remote marine free troposphere site: Implications for optical properties, Geophys. Res. Lett., 42, 1243–1250, https://doi.org/10.1002/2014GL062404, 2015.

Choobari, O. A., Zawar-Reza, P., and Sturman, A.: The global distribution of mineral dust and its impacts on the climate system: A review, Atmospheric Res., 138, 152–165, https://doi.org/10.1016/j.atmosres.2013.11.007, 2014.

Clarke, A. and Kapustin, V.: Hemispheric Aerosol Vertical Profiles: Anthropogenic Impacts on Optical Depth and Cloud Nuclei, Science, 329, 1488–1492, https://doi.org/10.1126/science.1188838, 2010.

Clarke, A., McNaughton, C., Kapustin, V., Shinozuka, Y., Howell, S., Dibb, J., Zhou, J., Anderson, B., Brekhovskikh, V., Turner, H., and Pinkerton, M.: Biomass burning and pollution aerosol over North America: Organic components and their influence on spectral optical properties and humidification response, J. Geophys. Res., 112, D12S18, https://doi.org/10.1029/2006JD007777, 2007.

Cooke, W. F., Jennings, S. G., and Spain, T. G.: Black carbon measurements at Mace Head, 1989-1996, J. Geophys. Res. Atmospheres, 102, 25339–25346, https://doi.org/10.1029/97JD01430, 1997.

Costabile, F., Barnaba, F., Angelini, F., and Gobbi, G. P.: Identification of key aerosol populations through their size and composition resolved spectral scattering and absorption, Atmospheric Chem. Phys., 13, 2455–2470, https://doi.org/10.5194/acp-13-2455-2013, 2013.

Cuevas, E., Gómez-Peláez, A. J., Rodríguez, S., Terradellas, E., Basart, S., García, R. D., García, O. E., and Alonso-Pérez, S.: The pulsating nature of large-scale Saharan dust transport as a result of interplays between mid-latitude Rossby waves and the North African Dipole Intensity, Atmos. Environ., 167, 586–602, https://doi.org/10.1016/j.atmosenv.2017.08.059, 2017.

Dadashazar, H., Painemal, D., Alipanah, M., Brunke, M., Chellappan, S., Corral, A. F., Crosbie, E., Kirschler, S., Liu, H., Moore, R. H., Robinson, C., Scarino, A. J., Shook, M., Sinclair, K., Thornhill, K. L., Voigt, C., Wang, H., Winstead, E., Zeng, X., Ziemba, L., Zuidema, P., and Sorooshian, A.: Cloud drop number concentrations over the western North Atlantic Ocean: seasonal cycle, aerosol interrelationships, and other influential factors, Atmospheric Chem. Phys., 21, 10499–10526, https://doi.org/10.5194/acp-21-10499-2021, 2021.

Dentener, F., Kinne, S., Bond, T., Boucher, O., Cofala, J., Generoso, S., Ginoux, P., Gong, S., Hoelzemann, J. J., Ito, A., Marelli, L., Penner, J. E., Putaud, J.-P., Textor, C., Schulz, M., van der Werf, G. R., and Wilson, J.: Emissions of primary aerosol and precursor gases in the years 2000 and 1750 prescribed data-sets for AeroCom, Atmospheric Chem. Phys., 6, 4321–4344, https://doi.org/10.5194/acp-6-4321-2006, 2006.

Dong, X., Xi, B., Kennedy, A., Minnis, P., and Wood, R.: A 19-Month Record of Marine Aerosol–Cloud–Radiation Properties Derived from DOE ARM Mobile Facility Deployment at the Azores. Part I: Cloud Fraction and Single-Layered MBL Cloud Properties, J. Clim., 27, 3665–3682, https://doi.org/10.1175/JCLI-D-13-00553.1, 2014.

Dzepina, K., Mazzoleni, C., Fialho, P., China, S., Zhang, B., Owen, R. C., Helmig, D., Hueber, J., Kumar, S., Perlinger, J. A., Kramer, L. J., Dziobak, M. P., Ampadu, M. T., Olsen, S., Wuebbles, D. J., and Mazzoleni, L. R.: Molecular characterization of free tropospheric aerosol collected at the Pico Mountain Observatory: a case study with a long-range transported biomass burning plume, Atmospheric Chem. Phys., 15, 5047–5068, https://doi.org/10.5194/acp-15-5047-2015, 2015.

Facchini, M. C., Rinaldi, M., Decesari, S., Carbone, C., Finessi, E., Mircea, M., Fuzzi, S., Ceburnis, D., Flanagan, R., Nilsson, E. D., de Leeuw, G., Martino, M., Woeltjen, J., and O'Dowd, C. D.: Primary submicron marine aerosol dominated by insoluble organic colloids and aggregates, Geophys. Res. Lett., 35, L17814, https://doi.org/10.1029/2008GL034210, 2008.

Fan, J., Wang, Y., Rosenfeld, D., and Liu, X.: Review of Aerosol–Cloud Interactions: Mechanisms, Significance, and Challenges, J. Atmospheric Sci., 73, 4221–4252, https://doi.org/10.1175/JAS-D-16-0037.1, 2016.

Feingold, G. and McComiskey, A.: ARM's Aerosol–Cloud–Precipitation Research (Aerosol Indirect Effects), Meteorol. Monogr., 57, 22.1-22.15, https://doi.org/10.1175/AMSMONOGRAPHS-D-15-0022.1, 2016.

Friese, C. A., van der Does, M., Merkel, U., Iversen, M. H., Fischer, G., and Stuut, J.-B. W.: Environmental factors controlling the seasonal variability in particle size distribution of modern Saharan dust deposited off Cape Blanc, Aeolian Res., 22, 165–179, https://doi.org/10.1016/j.aeolia.2016.04.005, 2016.

Gallo, F., Uin, J., Springston, S., Wang, J., Zheng, G., Kuang, C., Wood, R., Azevedo, E. B., McComiskey, A., Mei, F., Theisen, A., Kyrouac, J., and Aiken, A. C.: Identifying a regional aerosol baseline in the eastern North Atlantic using collocated measurements and a mathematical algorithm to mask high-submicron-number-concentration aerosol events, Atmospheric Chem. Phys., 20, 7553–7573, https://doi.org/10.5194/acp-20-7553-2020, 2020.

García, M. I., Rodríguez, S., and Alastuey, A.: Impact of North America on the aerosol composition in the North Atlantic free troposphere, Atmospheric Chem. Phys., 17, 7387–7404, https://doi.org/10.5194/acp-17-7387-2017, 2017.

Garrett, T. J. and Hobbs, P. V.: Long-Range Transport of Continental Aerosols over the Atlantic Ocean and Their Effects on Cloud Structures, J. Atmospheric Sci., 52, 2977–2984, https://doi.org/10.1175/1520-0469(1995)052<2977:LRTOCA>2.0.CO;2, 1995.

Haynes, W.: Tukey's Test, in: Encyclopedia of Systems Biology, edited by: Dubitzky, W., Wolkenhauer, O., Cho, K.-H., and Yokota, H., Springer New York, New York, NY, 2303–2304, https://doi.org/10.1007/978-1-4419-9863-7_1212, 2013.

Honrath, R. E.: Regional and hemispheric impacts of anthropogenic and biomass burning emissions on summertime CO and O_3 in the North Atlantic lower free troposphere, J. Geophys. Res., 109, D24310, https://doi.org/10.1029/2004JD005147, 2004.

Honrath, R. E., Owen, R. C., Val Martín, M., Seid, J. S., Lapina, K., Fialho, P., Dziobak, M. P., Kleissl, J., and Westphal, D. L.: Regional and hemispheric impacts of anthropogenic and biomass burning emissions on summertime CO and O_3 in the North Atlantic lower free troposphere, J. Geophys. Res., 109, D24310, https://doi.org/10.1029/2004JD005147, 2004.

Hosseini, S., Li, Q., Cocker, D., Weise, D., Miller, A., Shrivastava, M., Miller, J. W., Mahalingam, S., Princevac, M., and Jung, H.: Particle size distributions from laboratory-scale biomass fires using fast response instruments, Atmospheric Chem. Phys., 10, 8065–8076, https://doi.org/10.5194/acp-10-8065-2010, 2010.

Hudson, J. G. and Xie, Y.: Vertical distributions of cloud condensation nuclei spectra over the summertime northeast Pacific and Atlantic Oceans, J. Geophys. Res. Atmospheres, 104, 30219–30229, https://doi.org/10.1029/1999JD900413, 1999.

Janhäll, S., Andreae, M. O., and Pöschl, U.: Biomass burning aerosol emissions from vegetation fires: particle number and mass emission factors and size distributions, Atmospheric Chem. Phys., 10, 1427–1439, https://doi.org/10.5194/acp-10-1427-2010, 2010.

Junker, C., Jennings, S. G., and Cachier, H.: Aerosol light absorption in the North Atlantic: trends and seasonal characteristics during the period 1989 to 2003, Atmospheric Chem. Phys., 6, 1913–1925, https://doi.org/10.5194/acp-6-1913-2006, 2006.

Kalashnikova, O. V. and Kahn, R. A.: Mineral dust plume evolution over the Atlantic from MISR and MODIS aerosol retrievals, J. Geophys. Res., 113, D24204, https://doi.org/10.1029/2008JD010083, 2008.

Khaykin, S. M., Godin-Beekmann, S., Hauchecorne, A., Pelon, J., Ravetta, F., and Keckhut, P.: Stratospheric Smoke With Unprecedentedly High Backscatter Observed by Lidars Above Southern France, Geophys. Res. Lett., 45, 1639–1646, https://doi.org/10.1002/2017GL076763, 2018.

Kleefeld, C.: Relative contribution of submicron and supermicron particles to aerosol light scattering in the marine boundary layer, J. Geophys. Res., 107, 8103, https://doi.org/10.1029/2000JD000262, 2002.

Kloss, C., Berthet, G., Sellitto, P., Ploeger, F., Bucci, S., Khaykin, S., Jégou, F., Taha, G., Thomason, L. W., Barret, B., Le Flochmoen, E., von Hobe, M., Bossolasco, A., Bègue, N., and Legras, B.: Transport of the 2017 Canadian wildfire plume to the tropics via the Asian monsoon circulation, Atmospheric Chem. Phys., 19, 13547–13567, https://doi.org/10.5194/acp-19-13547-2019, 2019.

Koehler, K. A., Kreidenweis, S. M., DeMott, P. J., Petters, M. D., Prenni, A. J., and Carrico, C. M.: Hygroscopicity and cloud droplet activation of mineral dust aerosol, Geophys. Res. Lett., 36, L08805, https://doi.org/10.1029/2009GL037348, 2009.

Kolstad, E. W., Bracegirdle, T. J., and Seierstad, I. A.: Marine cold-air outbreaks in the North Atlantic: temporal distribution and associations with large-scale atmospheric circulation, Clim. Dyn., 33, 187–197, https://doi.org/10.1007/s00382-008-0431-5, 2009.

Korhonen, H., Carslaw, K. S., Spracklen, D. V., Mann, G. W., and Woodhouse, M. T.: Influence of oceanic dimethyl sulfide emissions on cloud condensation nuclei concentrations and seasonality over the remote Southern Hemisphere oceans: A global model study, J. Geophys. Res., 113, D15204, https://doi.org/10.1029/2007JD009718, 2008.

Korolev, A. V. and Mazin, I. P.: Supersaturation of Water Vapor in Clouds, J. Atmospheric Sci., 60, 2957–2974, https://doi.org/10.1175/1520-0469(2003)060<2957:SOWVIC>2.0.CO;2, 2003.

Kuang, C., Mei, F., Pacific Northwest National Laboratory, Brookhaven National Laboratory, Argonne National Laboratory, and Oak Ridge National Laboratory: Condensation Particle Counter (CPC) Instrument Handbook - Airborne Version, https://doi.org/10.2172/1562676, 2019.

Laken, B. A., Parviainen, H., Pallé, E., and Shahbaz, T.: Saharan mineral dust outbreaks observed over the North Atlantic island of La Palma in summertime between 1984 and 2012: Summertime Saharan Dust Outbreaks over La Palma, Q. J. R. Meteorol. Soc., 140, 1058–1068, https://doi.org/10.1002/qj.2170, 2014.

Lapina, K., Heald, C. L., Spracklen, D. V., Arnold, S. R., Allan, J. D., Coe, H., McFiggans, G., Zorn, S. R., Drewnick, F., Bates, T. S., Hawkins, L. N., Russell, L. M., Smirnov, A., O'Dowd, C. D., and Hind, A. J.: Investigating organic aerosol loading in the remote marine environment, Atmospheric Chem. Phys., 11, 8847–8860, https://doi.org/10.5194/acp-11-8847-2011, 2011.

Lathem, T. L., Beyersdorf, A. J., Thornhill, K. L., Winstead, E. L., Cubison, M. J., Hecobian, A., Jimenez, J. L., Weber, R. J., Anderson, B. E., and Nenes, A.: Analysis of CCN activity of Arctic aerosol and Canadian biomass burning during summer 2008, Atmospheric Chem. Phys., 13, 2735–2756, https://doi.org/10.5194/acp-13-2735-2013, 2013.

Lawrence, C. R. and Neff, J. C.: The contemporary physical and chemical flux of aeolian dust: A synthesis of direct measurements of dust deposition, Chem. Geol., 267, 46–63, https://doi.org/10.1016/j.chemgeo.2009.02.005, 2009.

Levin, E. J. T., McMeeking, G. R., Carrico, C. M., Mack, L. E., Kreidenweis, S. M., Wold, C. E., Moosmüller, H., Arnott, W. P., Hao, W. M., Collett, J. L., and Malm, W. C.: Biomass burning smoke aerosol properties measured during Fire Laboratory at Missoula Experiments (FLAME), J. Geophys. Res., 115, D18210, https://doi.org/10.1029/2009JD013601, 2010.

Liu, J., Li, Z., and Cribb, M.: Response of Marine Boundary Layer Cloud Properties to Aerosol Perturbations Associated with Meteorological Conditions from the 19-Month AMF-Azores Campaign, J. Atmospheric Sci., 73, 4253–4268, https://doi.org/10.1175/JAS-D-15-0364.1, 2016.

Logan, T., Xi, B., and Dong, X.: Aerosol properties and their influences on marine boundary layer cloud condensation nuclei at the ARM mobile facility over the Azores: Aerosol and influences on MBL CCN, J. Geophys. Res. Atmospheres, 119, 4859–4872, https://doi.org/10.1002/2013JD021288, 2014a.

Lopez-Yglesias, X. F., Yeung, M. C., Dey, S. E., Brechtel, F. J., and Chan, C. K.: Performance Evaluation of the Brechtel Mfg. Humidified Tandem Differential Mobility Analyzer (BMI HTDMA) for Studying Hygroscopic Properties of Aerosol Particles, Aerosol Sci. Technol., 48, 969–980, https://doi.org/10.1080/02786826.2014.952366, 2014.

Mahowald, N., Albani, S., Kok, J. F., Engelstaeder, S., Scanza, R., Ward, D. S., and Flanner, M. G.: The size distribution of desert dust aerosols and its impact on the Earth system, Aeolian Res., 15, 53–71, https://doi.org/10.1016/j.aeolia.2013.09.002, 2014.

Maring, H.: Mineral dust aerosol size distribution change during atmospheric transport, J. Geophys. Res., 108, 8592, https://doi.org/10.1029/2002JD002536, 2003.

Mather, J. H. and Voyles, J. W.: The Arm Climate Research Facility: A Review of Structure and Capabilities, Bull. Am. Meteorol. Soc., 94, 377–392, https://doi.org/10.1175/BAMS-D-11-00218.1, 2013.

Moore, R. H., Karydis, V. A., Capps, S. L., Lathem, T. L., and Nenes, A.: Droplet number uncertainties associated with CCN: an assessment using observations and a global model adjoint, Atmospheric Chem. Phys., 13, 4235–4251, https://doi.org/10.5194/acp-13-4235-2013, 2013.

Mungall, E. L., Abbatt, J. P. D., Wentzell, J. J. B., Lee, A. K. Y., Thomas, J. L., Blais, M., Gosselin, M., Miller, L. A., Papakyriakou, T., Willis, M. D., and Liggio, J.: Microlayer source of oxygenated volatile organic compounds in the summertime marine Arctic boundary layer, Proc. Natl. Acad. Sci., 114, 6203–6208, https://doi.org/10.1073/pnas.1620571114, 2017.

5 Nakamae, K. and Shiotani, M.: Interannual variability in Saharan dust over the North Atlantic Ocean and its relation to meteorological fields during northern winter, Atmospheric Res., 122, 336–346, https://doi.org/10.1016/j.atmosres.2012.09.012, 2013.

O'Dowd, C., Ceburnis, D., Ovadnevaite, J., Vaishya, A., Rinaldi, M., and Facchini, M. C.: Do anthropogenic, continental or coastal aerosol sources impact on a marine aerosol signature at Mace Head?, Atmospheric Chem. Phys., 14, 10687–10704, 10 https://doi.org/10.5194/acp-14-10687-2014, 2014.

O'Dowd, C. D., Smith, M. H., Consterdine, I. E., and Lowe, J. A.: Marine aerosol, sea-salt, and the marine sulphur cycle: a short review, Atmos. Environ., 31, 73–80, https://doi.org/10.1016/S1352-2310(96)00106-9, 1997.

O'Dowd, C. D., Facchini, M. C., Cavalli, F., Ceburnis, D., Mircea, M., Decesari, S., Fuzzi, S., Yoon, Y. J., and Putaud, J.-P.: Biogenically driven organic contribution to marine aerosol, Nature, 431, 676–680, https://doi.org/10.1038/nature02959, 2004.

15 Omar, A. H., Winker, D. M., Vaughan, M. A., Hu, Y., Trepte, C. R., Ferrare, R. A., Lee, K.-P., Hostetler, C. A., Kittaka, C., Rogers, R. R., Kuehn, R. E., and Liu, Z.: The CALIPSO Automated Aerosol Classification and Lidar Ratio Selection Algorithm, J. Atmospheric Ocean. Technol., 26, 1994–2014, https://doi.org/10.1175/2009JTECHA1231.1, 2009.

Owen, R. C., Cooper, O. R., Stohl, A., and Honrath, R. E.: An analysis of the mechanisms of North American pollutant transport to the central North Atlantic lower free troposphere: LOWER FREE TROPOSPHERE EXPORT MECHANISMS, 20 J. Geophys. Res. Atmospheres, 111, https://doi.org/10.1029/2006JD007062, 2006.

Pandis, S. N., Russell, L. M., and Seinfeld, J. H.: The relationship between DMS flux and CCN concentration in remote marine regions, J. Geophys. Res., 99, 16945, https://doi.org/10.1029/94JD01119, 1994.

Pennypacker, S. and Wood, R.: A Case Study in Low Aerosol Number Concentrations Over the Eastern North Atlantic: Implications for Pristine Conditions in the Remote Marine Boundary Layer, J. Geophys. Res. Atmospheres, 122, 12,393-25 12,415, https://doi.org/10.1002/2017JD027493, 2017.

Peterson, D. A., Campbell, J. R., Hyer, E. J., Fromm, M. D., Kablick, G. P., Cossuth, J. H., and DeLand, M. T.: Wildfire-driven thunderstorms cause a volcano-like stratospheric injection of smoke, Npj Clim. Atmospheric Sci., 1, 30, https://doi.org/10.1038/s41612-018-0039-3, 2018.

Petters, M. D. and Kreidenweis, S. M.: A single parameter representation of hygroscopic growth and cloud condensation 30 nucleus activity, Atmospheric Chem. Phys., 7, 1961–1971, https://doi.org/10.5194/acp-7-1961-2007, 2007.

Petters, M. D., Carrico, C. M., Kreidenweis, S. M., Prenni, A. J., DeMott, P. J., Collett, J. L., and Moosmüller, H.: Cloud condensation nucleation activity of biomass burning aerosol, J. Geophys. Res., 114, D22205, https://doi.org/10.1029/2009JD012353, 2009.

Pohl, K., Cantwell, M., Herckes, P., and Lohmann, R.: Black carbon concentrations and sources in the marine boundary layer 35 of the tropical Atlantic Ocean using four methodologies, Atmospheric Chem. Phys., 14, 7431–7443, https://doi.org/10.5194/acp-14-7431-2014, 2014.

Quinn, P. K. and Bates, T. S.: The case against climate regulation via oceanic phytoplankton sulphur emissions, Nature, 480, 51–56, https://doi.org/10.1038/nature10580, 2011.

Quinn, P. K., Bates, T. S., Coffman, D. J., Upchurch, L., Johnson, J. E., Moore, R., Ziemba, L., Bell, T. G., Saltzman, E. S., 40 Graff, J., and Behrenfeld, M. J.: Seasonal Variations in Western North Atlantic Remote Marine Aerosol Properties, J. Geophys. Res. Atmospheres, 124, 14240–14261, https://doi.org/10.1029/2019JD031740, 2019.

Redemann, J., Wood, R., Zuidema, P., Doherty, S. J., Luna, B., LeBlanc, S. E., Diamond, M. S., Shinozuka, Y., Chang, I. Y., Ueyama, R., Pfister, L., Ryoo, J.-M., Dobracki, A. N., da Silva, A. M., Longo, K. M., Kacenelenbogen, M. S., Flynn, C. J., Pistone, K., Knox, N. M., Piketh, S. J., Haywood, J. M., Formenti, P., Mallet, M., Stier, P., Ackerman, A. S., Bauer, S. E., 45 Fridlind, A. M., Carmichael, G. R., Saide, P. E., Ferrada, G. A., Howell, S. G., Freitag, S., Cairns, B., Holben, B. N., Knobelspiesse, K. D., Tanelli, S., L'Ecuyer, T. S., Dzambo, A. M., Sy, O. O., McFarquhar, G. M., Poellot, M. R., Gupta, S., O'Brien, J. R., Nenes, A., Kacarab, M., Wong, J. P. S., Small-Griswold, J. D., Thornhill, K. L., Noone, D., Podolske, J. R., Schmidt, K. S., Pilewskie, P., Chen, H., Cochrane, S. P., Sedlacek, A. J., Lang, T. J., Stith, E., Segal-Rozenhaimer, M., Ferrare, R. A., Burton, S. P., Hostetler, C. A., Diner, D. J., Seidel, F. C., Platnick, S. E., Myers, J. S., Meyer, K. G., Spangenberg, D.

A., Maring, H., and Gao, L.: An overview of the ORACLES (ObseRvations of Aerosols above CLouds and their intEractionS) project: aerosol–cloud–radiation interactions in the southeast Atlantic basin, Atmospheric Chem. Phys., 21, 1507–1563, https://doi.org/10.5194/acp-21-1507-2021, 2021.

Rémillard, J., Kollias, P., Luke, E., and Wood, R.: Marine Boundary Layer Cloud Observations in the Azores, J. Clim., 25, 7381–7398, https://doi.org/10.1175/JCLI-D-11-00610.1, 2012.

Riemer, N., Doherty, O. M., and Hameed, S.: On the variability of African dust transport across the Atlantic, Geophys. Res. Lett., 33, L13814, https://doi.org/10.1029/2006GL026163, 2006.

Rinaldi, M., Decesari, S., Finessi, E., Giulianelli, L., Carbone, C., Fuzzi, S., O'Dowd, C. D., Ceburnis, D., and Facchini, M. C.: Primary and Secondary Organic Marine Aerosol and Oceanic Biological Activity: Recent Results and New Perspectives for Future Studies, Adv. Meteorol., 2010, 1–10, https://doi.org/10.1155/2010/310682, 2010.

Roberts, G., Mauger, G., Hadley, O., and Ramanathan, V.: North American and Asian aerosols over the eastern Pacific Ocean and their role in regulating cloud condensation nuclei, J. Geophys. Res., 111, D13205, https://doi.org/10.1029/2005JD006661, 2006.

Roberts, G. C. and Nenes, A.: A Continuous-Flow Streamwise Thermal-Gradient CCN Chamber for Atmospheric Measurements, Aerosol Sci. Technol., 39, 206–221, https://doi.org/10.1080/027868290913988, 2005.

Rose, D., Gunthe, S. S., Mikhailov, E., Frank, G. P., Dusek, U., Andreae, M. O., and Pöschl, U.: Calibration and measurement uncertainties of a continuous-flow cloud condensation nuclei counter (DMT-CCNC): CCN activation of ammonium sulfate and sodium chloride aerosol particles in theory and experiment, Atmospheric Chem. Phys., 8, 1153–1179, https://doi.org/10.5194/acp-8-1153-2008, 2008.

Rosenfeld, D., Andreae, M. O., Asmi, A., Chin, M., de Leeuw, G., Donovan, D. P., Kahn, R., Kinne, S., Kivekäs, N., Kulmala, M., Lau, W., Schmidt, K. S., Suni, T., Wagner, T., Wild, M., and Quaas, J.: Global observations of aerosol-cloud-precipitation-climate interactions: Aerosol-cloud-climate interactions, Rev. Geophys., 52, 750–808, https://doi.org/10.1002/2013RG000441, 2014.

Saliba, G., Chen, C., Lewis, S., Russell, L. M., Quinn, P. K., Bates, T. S., Bell, T. G., Lawler, M. J., Saltzman, E. S., Sanchez, K. J., Moore, R., Shook, M., Rivellini, L., Lee, A., Baetge, N., Carlson, C. A., and Behrenfeld, M. J.: Seasonal Differences and Variability of Concentrations, Chemical Composition, and Cloud Condensation Nuclei of Marine Aerosol Over the North Atlantic, J. Geophys. Res. Atmospheres, 125, https://doi.org/10.1029/2020JD033145, 2020.

Sanchez, K. J., Chen, C.-L., Russell, L. M., Betha, R., Liu, J., Price, D. J., Massoli, P., Ziemba, L. D., Crosbie, E. C., Moore, R. H., Müller, M., Schiller, S. A., Wisthaler, A., Lee, A. K. Y., Quinn, P. K., Bates, T. S., Porter, J., Bell, T. G., Saltzman, E. S., Vaillancourt, R. D., and Behrenfeld, M. J.: Substantial Seasonal Contribution of Observed Biogenic Sulfate Particles to Cloud Condensation Nuclei, Sci. Rep., 8, 3235, https://doi.org/10.1038/s41598-018-21590-9, 2018.

Sanchez, K. J., Zhang, B., Liu, H., Brown, M. D., Crosbie, E. C., Gallo, F., Hair, J. W., Hostetler, C. A., Jordan, C. E., Robinson, C. E., Scarino, A. J., Shingler, T. J., Shook, M. A., Thornhill, K. L., Wiggins, E. B., Winstead, E. L., Ziemba, L. D., Saliba, G., Lewis, S. L., Russell, L. M., Quinn, P. K., Bates, T. S., Porter, J., Bell, T. G., Gaube, P., Saltzman, E. S., Behrenfeld, M. J., and Moore, R. H.: North Atlantic Ocean SST-gradient-driven variations in aerosol and cloud evolution along Lagrangian cold-air outbreak trajectories, Atmospheric Chem. Phys., 22, 2795–2815, https://doi.org/10.5194/acp-22-2795-2022, 2022.

Seinfeld, J. H., Bretherton, C., Carslaw, K. S., Coe, H., DeMott, P. J., Dunlea, E. J., Feingold, G., Ghan, S., Guenther, A. B., Kahn, R., Kraucunas, I., Kreidenweis, S. M., Molina, M. J., Nenes, A., Penner, J. E., Prather, K. A., Ramanathan, V., Ramaswamy, V., Rasch, P. J., Ravishankara, A. R., Rosenfeld, D., Stephens, G., and Wood, R.: Improving our fundamental understanding of the role of aerosol–cloud interactions in the climate system, Proc. Natl. Acad. Sci., 113, 5781–5790, https://doi.org/10.1073/pnas.1514043113, 2016.

Shank, L. M., Howell, S., Clarke, A. D., Freitag, S., Brekhovskikh, V., Kapustin, V., McNaughton, C., Campos, T., and Wood, R.: Organic matter and non-refractory aerosol over the remote Southeast Pacific: oceanic and combustion sources, Atmospheric Chem. Phys., 12, 557–576, https://doi.org/10.5194/acp-12-557-2012, 2012.

Sharon, T. M., Albrecht, B. A., Jonsson, H. H., Minnis, P., Khaiyer, M. M., van Reken, T. M., Seinfeld, J., and Flagan, R.: Aerosol and Cloud Microphysical Characteristics of Rifts and Gradients in Maritime Stratocumulus Clouds, J. Atmospheric Sci., 63, 983–997, https://doi.org/10.1175/JAS3667.1, 2006.

Sorooshian, A., Corral, A. F., Braun, R. A., Cairns, B., Crosbie, E., Ferrare, R., Hair, J., Kleb, M. M., Hossein Mardi, A., Maring, H., McComiskey, A., Moore, R., Painemal, D., Scarino, A. J., Schlosser, J., Shingler, T., Shook, M., Wang, H., Zeng,

X., Ziemba, L., and Zuidema, P.: Atmospheric Research Over the Western North Atlantic Ocean Region and North American East Coast: A Review of Past Work and Challenges Ahead, J. Geophys. Res. Atmospheres, 125, https://doi.org/10.1029/2019JD031626, 2020.

Springston, S.: Particle Soot Absorption Photometer (PSAP) Instrument Handbook, https://doi.org/10.2172/1246162, 2018.

5   Stein, A. F., Draxler, R. R., Rolph, G. D., Stunder, B. J. B., Cohen, M. D., and Ngan, F.: NOAA's HYSPLIT Atmospheric Transport and Dispersion Modeling System, Bull. Am. Meteorol. Soc., 96, 2059–2077, https://doi.org/10.1175/BAMS-D-14-00110.1, 2015.

Tomlin, J. M., Jankowski, K. A., Veghte, D. P., China, S., Wang, P., Fraund, M., Weis, J., Zheng, G., Wang, Y., Rivera-Adorno, F., Raveh-Rubin, S., Knopf, D. A., Wang, J., Gilles, M. K., Moffet, R. C., and Laskin, A.: Impact of dry intrusion
10 events on the composition and mixing state of particles during the winter Aerosol and Cloud Experiment in the Eastern North Atlantic (ACE-ENA), Atmospheric Chem. Phys., 21, 18123–18146, https://doi.org/10.5194/acp-21-18123-2021, 2021.

Twomey, S.: Pollution and the planetary albedo, Atmospheric Environ. 1967, 8, 1251–1256, https://doi.org/10.1016/0004-6981(74)90004-3, 1974.

Uin, J.: 3002 Humidified Tandem Differential Mobility Analyzer Instrument Handbook, https://doi.org/10.2172/1251403,
15 2016.

Uin, J., Aiken, A. C., Dubey, M. K., Kuang, C., Pekour, M., Salwen, C., Sedlacek, A. J., Senum, G., Smith, S., Wang, J., Watson, T. B., and Springston, S. R.: Atmospheric Radiation Measurement (ARM) Aerosol Observing Systems (AOS) for Surface-Based In Situ Atmospheric Aerosol and Trace Gas Measurements, J. Atmospheric Ocean. Technol., 36, 2429–2447, https://doi.org/10.1175/JTECH-D-19-0077.1, 2019.

20 Vignati, E., Facchini, M. C., Rinaldi, M., Scannell, C., Ceburnis, D., Sciare, J., Kanakidou, M., Myriokefalitakis, S., Dentener, F., and O'Dowd, C. D.: Global scale emission and distribution of sea-spray aerosol: Sea-salt and organic enrichment, Atmos. Environ., 44, 670–677, https://doi.org/10.1016/j.atmosenv.2009.11.013, 2010.

Virkkula, A.: Correction of the Calibration of the 3-wavelength Particle Soot Absorption Photometer (3λ PSAP), Aerosol Sci. Technol., 44, 706–712, https://doi.org/10.1080/02786826.2010.482110, 2010.

25 Virkkula, A., Ahlquist, N. C., Covert, D. S., Arnott, W. P., Sheridan, P. J., Quinn, P. K., and Coffman, D. J.: Modification, Calibration and a Field Test of an Instrument for Measuring Light Absorption by Particles, Aerosol Sci. Technol., 39, 68–83, https://doi.org/10.1080/027868290901963, 2005.

Wang, J., Wood, R., Jensen, M. P., Chiu, J. C., Liu, Y., Lamer, K., Desai, N., Giangrande, S. E., Knopf, D. A., Kollias, P., Laskin, A., Liu, X., Lu, C., Mechem, D., Mei, F., Starzec, M., Tomlinson, J., Wang, Y., Yum, S. S., Zheng, G., Aiken, A. C.,
30 Azevedo, E. B., Blanchard, Y., China, S., Dong, X., Gallo, F., Gao, S., Ghate, V. P., Glienke, S., Goldberger, L., Hardin, J. C., Kuang, C., Luke, E. P., Matthews, A. A., Miller, M. A., Moffet, R., Pekour, M., Schmid, B., Sedlacek, A. J., Shaw, R. A., Shilling, J. E., Sullivan, A., Suski, K., Veghte, D. P., Weber, R., Wyant, M., Yeom, J., Zawadowicz, M., and Zhang, Z.: Aerosol and Cloud Experiments in the Eastern North Atlantic (ACE-ENA), Bull. Am. Meteorol. Soc., 1–51, https://doi.org/10.1175/BAMS-D-19-0220.1, 2021a.

35 Wang, Y., Zheng, G., Jensen, M., Knopf, D., Laskin, A., Matthews, A., Mechem, D., Mei, F., Moffet, R., Sedlacek, A., Shilling, J., Springston, S., Sullivan, A., Tomlinson, J., Veghte, D., Weber, R., Wood, R., Zawadowicz, M., and Wang, J.: Vertical profiles of trace gas and aerosol properties over the Eastern North Atlantic: Variations with season and synoptic condition, Aerosols/Field Measurements/Troposphere/Physics (physical properties and processes), https://doi.org/10.5194/acp-2021-300, 2021b.

40 Wood, R.: Stratocumulus Clouds, Mon. Weather Rev., 140, 2373–2423, https://doi.org/10.1175/MWR-D-11-00121.1, 2012.

Wood, R., Wyant, M., Bretherton, C. S., Rémillard, J., Kollias, P., Fletcher, J., Stemmler, J., Szoeke, S. de, Yuter, S., Miller, M., Mechem, D., Tselioudis, G., Chiu, J. C., Mann, J. A. L., O'Connor, E. J., Hogan, R. J., Dong, X., Miller, M., Ghate, V., Jefferson, A., Min, Q., Minnis, P., Palikonda, R., Albrecht, B., Luke, E., Hannay, C., and Lin, Y.: Clouds, Aerosols, and Precipitation in the Marine Boundary Layer: An Arm Mobile Facility Deployment, Bull. Am. Meteorol. Soc., 96, 419–440,
45 https://doi.org/10.1175/BAMS-D-13-00180.1, 2015.

Yoon, Y. J., Ceburnis, D., Cavalli, F., Jourdan, O., Putaud, J. P., Facchini, M. C., Decesari, S., Fuzzi, S., Sellegri, K., Jennings, S. G., and O'Dowd, C. D.: Seasonal characteristics of the physicochemical properties of North Atlantic marine atmospheric aerosols, J. Geophys. Res., 112, D04206, https://doi.org/10.1029/2005JD007044, 2007.

Zellner, R.: [No title found], J. Atmospheric Chem., 37, 212–214, https://doi.org/10.1023/A:1006483708571, 2000.

Zhang, B., Owen, R. C., Perlinger, J. A., Helmig, D., Val Martín, M., Kramer, L., Mazzoleni, L. R., and Mazzoleni, C.: Ten-year chemical signatures associated with long-range transport observed in the free troposphere over the central North Atlantic, Elem. Sci. Anthr., 5, 8, https://doi.org/10.1525/elementa.194, 2017.

Zhang, X., Massoli, P., Quinn, P. K., Bates, T. S., and Cappa, C. D.: Hygroscopic growth of submicron and supermicron
5   aerosols   in   the   marine   boundary   layer,   J.   Geophys.   Res.   Atmospheres,   119,   8384–8399, https://doi.org/10.1002/2013JD021213, 2014.

Zhao, T. L., Gong, S. L., Huang, P., and Lavoué, D.: Hemispheric transport and influence of meteorology on global aerosol climatology, Atmospheric Chem. Phys., 12, 7609–7624, https://doi.org/10.5194/acp-12-7609-2012, 2012.

Zheng, G., Wang, Y., Aiken, A. C., Gallo, F., Jensen, M. P., Kollias, P., Kuang, C., Luke, E., Springston, S., Uin, J., Wood,
10   R., and Wang, J.: Marine boundary layer aerosol in the eastern North Atlantic: seasonal variations and key controlling processes, Atmospheric Chem. Phys., 18, 17615–17635, https://doi.org/10.5194/acp-18-17615-2018, 2018.

Zheng, G., Sedlacek, A. J., Aiken, A. C., Feng, Y., Watson, T. B., Raveh-Rubin, S., Uin, J., Lewis, E. R., and Wang, J.: Long-range transported North American wildfire aerosols observed in marine boundary layer of eastern North Atlantic, Environ. Int., 139, 105680, https://doi.org/10.1016/j.envint.2020.105680, 2020.

15   Zheng, G., Wang, Y., Wood, R., Jensen, M. P., Kuang, C., McCoy, I. L., Matthews, A., Mei, F., Tomlinson, J. M., Shilling, J. E., Zawadowicz, M. A., Crosbie, E., Moore, R., Ziemba, L., Andreae, M. O., and Wang, J.: New particle formation in the remote marine boundary layer, Nat. Commun., 12, 527, https://doi.org/10.1038/s41467-020-20773-1, 2021.

Tables and figures

Table 1. Aerosol Observing System measurements at ENA ARM site analyzed in this study.

Measurement	Symbol	Unit	Instrument	Refrence
Submicron aerosol number concentration	N_{tot}	cm^{-3}	Condensation Particle Counter CPC Model 3772, TSI Inc.	(Kuang et al., 2019)
Size distribution of submicron aerosols (70 to 1000 nm)		cm^{-3}	Ultra-High-Sensitivity Aerosol Spectometer UHSAS, DMT	(Uin, 2016b)
Number concentration of cloud condensation nuclei	CCN	cm^{-3}	Cloud Condensation Nuclei Counter CCN Model CCN-100, DMT	(Roberts and Nenes, 2005; Rose et al., 2008)
Aerosol growth factor			Humidified Tandem Differential Mobility Analyzer HTDMA Model 3002, Bretchel	(Lopez-Yglesias et al., 2014; Uin, 2016)
Aerosol absorption coefficients	B_{abs}	Mm^{-1}	Particle Soot Absorption Photometer PSAP 3-λ, Radiant Research	(Bond et al., 1999; Virkkula et al., 2005; Virkkula, 2010)
Aerosol scattering coefficients	B_{sca}	Mm^{-1}	Integrating Nephelometer Neph, Model 3563, TSI	(Costabile et al., 2013)

5   **Table 2.** Summary of multiday transported aerosol plumes events that affected ENA in 2017 including duration, aerosol emission origins, CALIPSO classification. The values of the three aerosol properties used by the algorithm to detect the events (median concentration of particles with D_p 100-1000 nm, median SSA 1 μm at λ 464 nm, and mean BC values) are shown in the rightmost column during each event (first line) and under baseline condition (in italic, second line).

Event	Duration (hours)	Origin (Hysplit)	CALIPSO aerosol classification	Median concentration particles D_p100-1000 nm	Median SSA 1 μm (λ 464 nm)	Mean BC (ng m^{-3})
January 07 to 11	114	Northern Europe	Mixture of dust, polluted continental aerosols and smoke	365 cm^{-3} *83 cm^{-3}*	0.87 *0.96*	229 ± 41 ng m^{-3} *36 ± 21 ng m^{-3}*
March 12 to 15	72	Artic/Canada	Mixture of dust, and marine aerosols	319 cm^{-3} *91 cm^{-3}*	0.93 *0.96*	115 ± 37 ng m^{-3} *35 ± 19 ng m^{-3}*
April 20 to 22	54	Northern Europe	Mixture of marine and polluted continental aerosols, and smoke	460 cm^{-3} *99 cm^{-3}*	0.94 *0.95*	121 ± 27 ng m^{-3} *29 ± 21 ng m^{-3}*
May 21 to 22	36	North America	Polluted continental aerosol and smoke	608 cm^{-3} *93 cm^{-3}*	0.94 *0.97*	142 ± 16 ng m^{-3} *33 ± 20 ng m^{-3}*
August 26 to 29	84	North America	Elevated smoke	332 cm^{-3} *105 cm^{-3}*	0.94 *0.95*	181 ± 58 ng m^{-3} *40 ± 25 ng m^{-3}*
September 09 to 13	96	North America/Canada	Data not available	289 cm^{-3} *103 cm^{-3}*	0.93 *0.96*	175 ± 39 ng m^{-3} *39 ± 22 ng m^{-3}*
October 11 to 13	48	Hurricane Ophelia	Mixture of dust, marine and polluted continental aerosols, and smoke	329 cm^{-3} *99 cm^{-3}*	0.89 *0.96*	144 ± 69 ng m^{-3} *30 ± 19 ng m^{-3}*
November 26 to28	54	North Africa	Mixture of dust, and marine aerosols	271 cm^{-3} *81 cm^{-3}*	0.91 *0.96*	181 ± 29 ng m^{-3} *34 ± 21 ng m^{-3}*
December 07 to 10	84	North Africa	Mixture of dust, and marine aerosols	235 cm^{-3} *80 cm^{-3}*	0.92 *0.96*	103 ± 18 ng m^{-3} *26 ± 18 ng m^{-3}*

10   Table 3. Summary of the characteristics of each type of multiday aerosol plume transport event

Dust and Marine mixture	Polluted continental and Marine mixture	Biomass burining
Statistically significant change in N_{tot} N_{tot} increase > 110%	Statistically significant change in N_{tot} N_{tot} increase between 95% and 110%	Statistically non-significant change in N_{tot} N_{tot} increase < 25%
statistically non-significant shift in size (N_{At} / N_{Ac}) N_{At} / N_{Ac} change < 1% N_{At} contribution to N_{tot} ~ 59% N_{At} contribution to N_{tot} ~ 38%	Statistically significant shift in size (N_{At} / N_{Ac}) N_{At} / N_{Ac} change > 200% N_{At} contribution to N_{tot} ~ 42% N_{At} contribution to N_{tot} ~ 56%	Statistically significant shift in size (N_{At} / N_{Ac}) N_{At} / N_{Ac} change > 200% N_{At} contribution to N_{tot} ~ 33% N_{At} contribution to N_{tot} ~ 63%
Statistically non-significant change in CCN potential Activation fraction $AF_{0.1\%}$ increase ~ 5%, $AF_{0.2\%}$ increase ~ 9%	Statistically significant change in CCN potential activation fraction $AF_{0.1\%}$ increase between 30% and 75% $AF_{0.2\%}$ increase between 35% and 100%	Statistically significant change in CCN potential activation fraction $AF_{0.1\%}$ and $AF_{0.2\%}$ increase > 75%
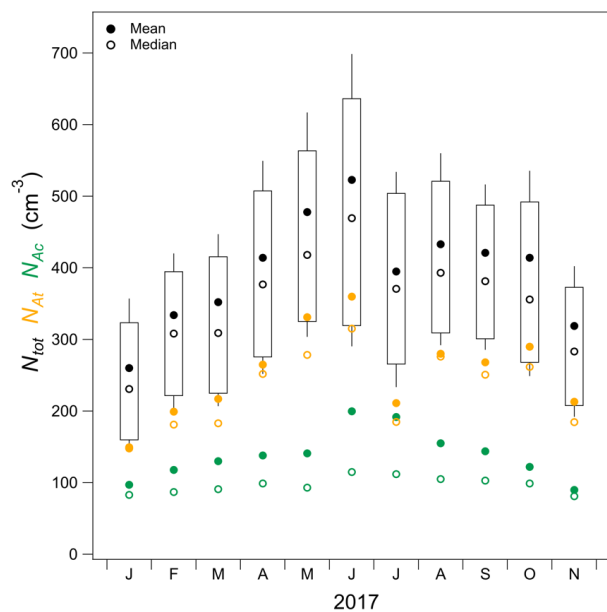
Figure 1. Box and whisker plot of monthly ubmicron aerosol number concentrations (box bottom at 25%, box top at 75%, whisker bottom at 10%, and whisker top at 90%). Mean (circles) and median (open circles) of total number concentration (black), number of Aitken (yellow), and accumulation (green) modes.
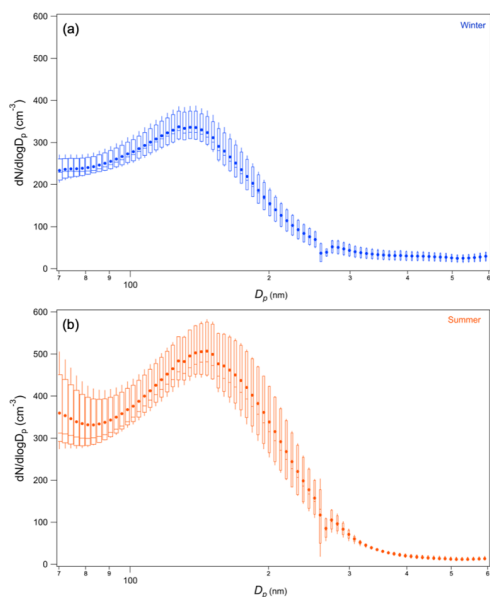
Figure 2. Particle size distribution in winter (a) and summer (b) 2017, per each size bean mean circle, and median -, box bottom at 25%, box top at 75%, whisker bottom at 10%, and whisker top at 90%). Discontinuity at around 270 nm due to UHSAS (handoff region between two internal gain stages).
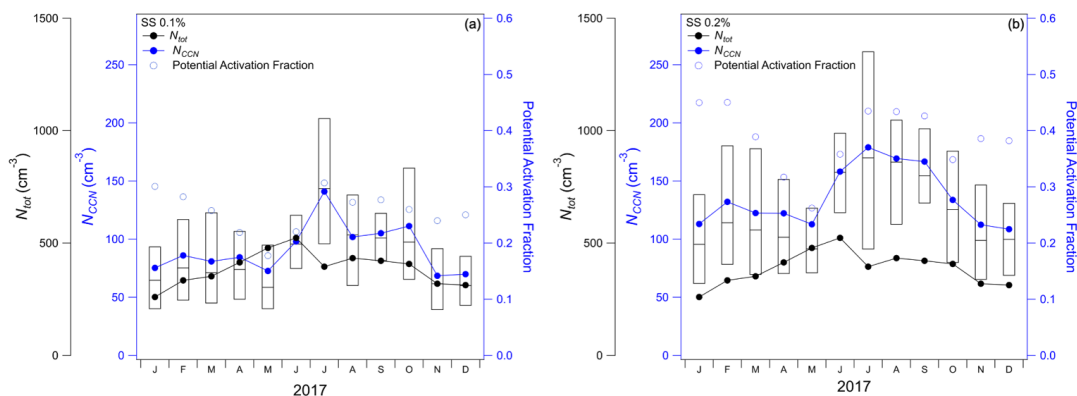
Figure 3. Box and whisker plot of $N_{CCN,0.1\%}$ (a) and $N_{CCN,0.2\%}$ (b), mean N_{CCN} blue circles, median -, box bottom at 25%, box top at 75%, whisker bottom at 10%, and whisker top at 90%, mean N_{tot}, black circles, and CCN potential activation fraction blue open circles.
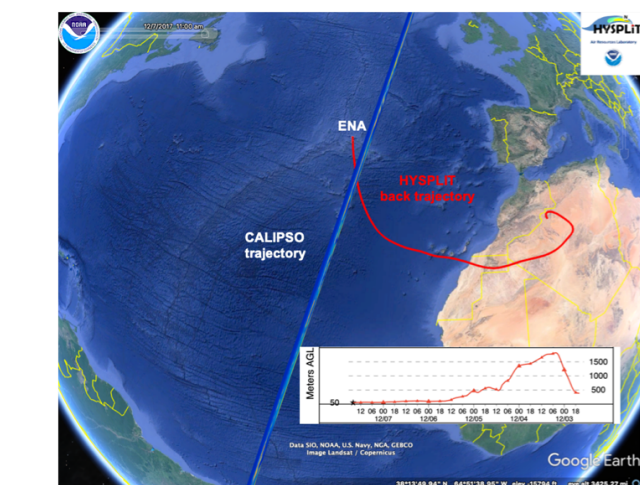
Figure 4. CALIPSO trajectories (blue) and Hysplit back trajectories (red) arriving at 50 m a.g.l. above the ENA site on December 07, 2017 (© Google Earth 2015).
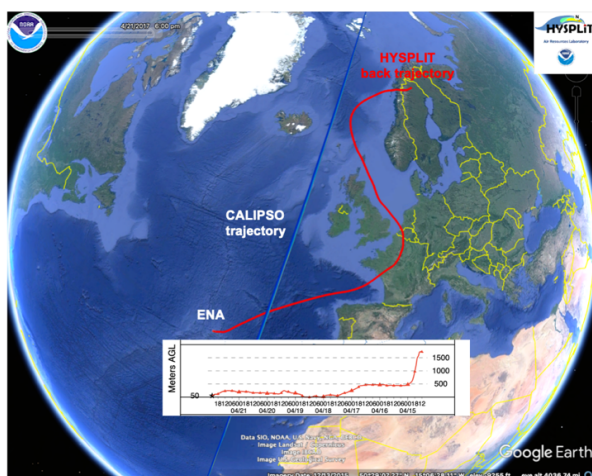
Figure 5. CALIPSO trajectories (blue), and Hysplit back trajectories (red) arriving at 50 m a.g.l. above the ENA site on April 21, 2017 (© Google Earth 2015).
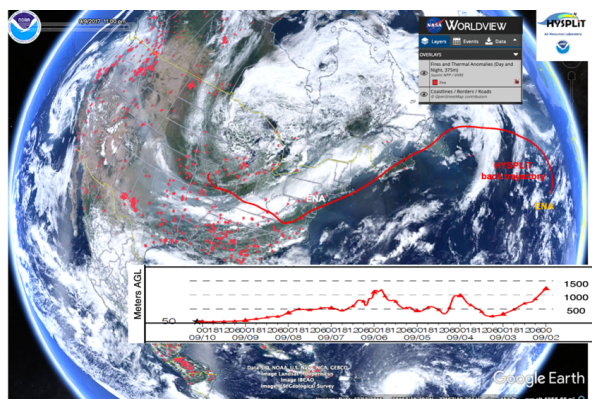
5   **Figure 6.** NASA Worldview VIIRS 375 Active fires between September 1 and 15, 2017 (red circles), and Hysplit back trajectories arriving at 50 m a.g.l. above the ENA site on September 10, 2017 (© Google Earth 2015).
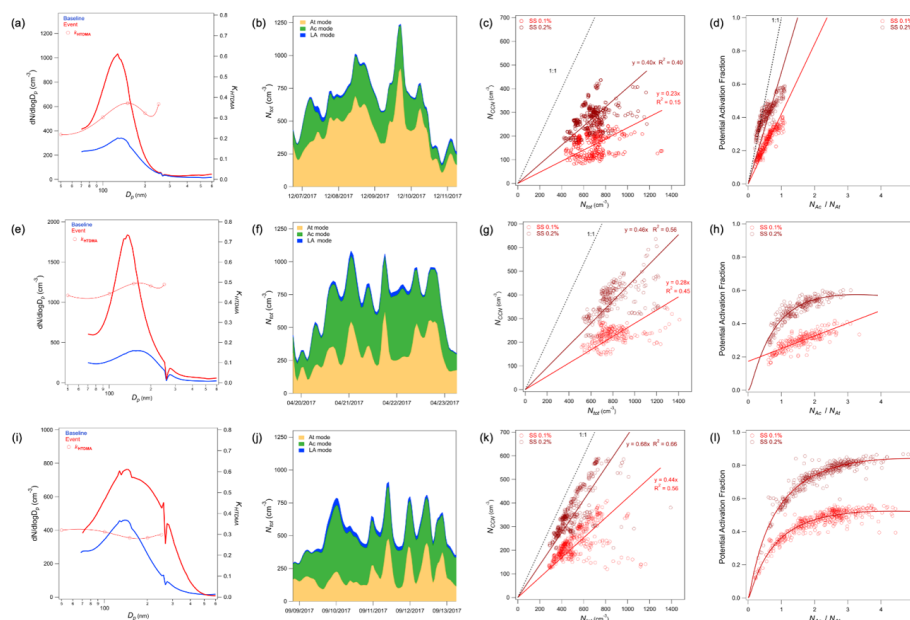
Figure 7. Case study of December 2017 (a to d), April 2017 (e to h), and September 2017 (i to l) events. Submicron particle size distribution
10   under baseline conditions (blue) and during the events (red), and κ_{HTDMA} (open circles) during the events (a, e, i), At, Ac, and LA mode contributions to (b, f, j), scatter plot of N_{CCN} versus N_{tot} during the event (red circle) and fitting lines for the events at SS 0.1% (red) and at SS 0.2% (dark red) (c, g, k), plot of potential activation ratio versus N_{Ac} / N_{At}, or the events at SS 0.1% (red) and at SS 0.2% (dark red) (d, h, l).
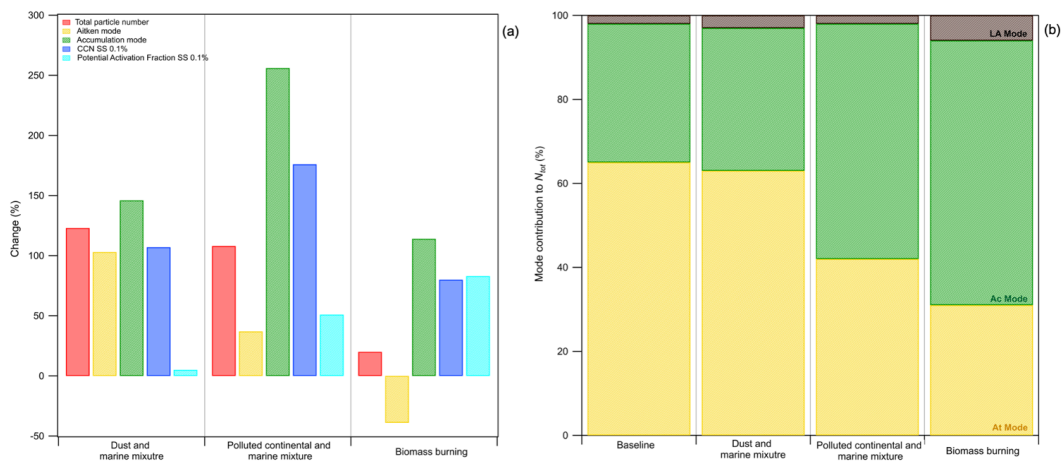
Figure 8. Mean percentage change in N_{tot}, N_{At}, N_{Ac}, $N_{CCN-0.1\%}$, and CCN potential activation fraction at SS 0.1% for each type of event (a); At, Ac and LA particle modes relative contribution to N_{tot}, for baseline and each type of event.